# Quantum thermodynamics explorations with a Hubbard-Holstein dimer

**Emil Östberg**


LUNDS UNIVERSITET

Supervisor: Claudio Verdozzi
Co-supervisor: Irene D'Amico

*Thesis submitted for the degree of bachelor (15 hp)*

Department of Physics
Division of Mathematical Physics

June 16, 2021

# Acknowledgments

First of all I would like to thank supervisor Claudio for always being available and always guiding me in the correct direction. I want to thank him for this great project, but also for teaching my lots of physics outside the project. He gave many other more general tips (besides the science) for my future career. My co-supervisor Irene showed great interest in my thesis and my results, she was much more involved than I expected. For this I'm very grateful. Most importantly, Claudio and Irene were always pleasant to interact with, and they would very often tell jokes.
Finally, I would to thank my friends both in Lund and in Uppsala: Axel, Erik, Hector, Martin, Erik, Jesper, Johan, Carl, Viktor, Albin, Erik, KJ and Samuel. I am grateful for the good times I spent discussing problems with my friends in Lund, some even contained in this thesis. I also would like to thank my friends in Uppsala for the grammatical-tips. Without these people studying during Covid-19 would have been very boring.

# Abstract

The goal of this project is to characterize the quantum thermodynamics of a Hubbard-Holstein dimer. We explore how the standard formalism of quantum thermodynamics behaves in the context many-body physics. To this end, the simplest possible lattice model which includes electron and electron-phonon interactions is used, namely the Hubbard-Holstein dimer. The system is time evolved using exact diagonalization, the Suzuki-Trotter method and the Lanczos method. We prepare various parts of the system in an initial thermal bath. We then compare the work to a case that does not include phonons. Three thermodynamic cases are realized: a battery, a few paths in phase space and a thermodynamic cycle. The results show that the effect of phonons is to smoothen out the features in the work distribution. We have seen that the battery can be charged, by increasing the amount of phonons. The path in phase space showed a path dependence, as we expected from classical thermodynamics. Finally, we have seen that the cycle experiences irreversibility by exhibiting hysteresis.

# Contents

# List of abbreviations

DFT- Density Functional Theory
HH - Hubbard-Holstein
QTD - Quantum thermodynamics
ED - exact diagonalization
ST - Suzuki-Trotter

# 1 Introduction and Background

In the beginning of the 20th century physicists thought they had a good grasp on the laws of nature: The movement of celestial bodies had been explained by Newton and the mysteries of electromagnetism had been summarized by Maxwell into four elegant equations.
However, some things did not make sense. Statistical physics predicted that the intensity of so-called black bodies diverges for small wavelengths, as the intensity becomes infinitely large. Planets and stars are examples of systems that are modeled as black bodies. Divergent quantities is not physical, as an infinite amount of radiated power does not obey energy conservation, nor does it agree with the observed spectrum. The baffling contradiction was called the ultraviolet catastrophe.
Moreover, the phenomenon called "photoelectric effect" had been unexplained for a long time. The photoelectric effect is essentially the emission of electrons when light is shone on a surface. Classical electromagnetism predicts that the emittance of electrons is a function of the intensity of the incoming light, furthermore even if the intensity is low one expects that eventually electrons will be emitted due to the accumulation of energy. Experiments showed strikingly different results. No electrons were emitted below a certain threshold in light frequency, independent of intensity, and above the threshold in frequency the emittance depended on the intensity.
The first hints towards the quantum nature of the universe was given by the solution to these problems. Max Planck solved the ultraviolet catastrophe by postulating that light only could be emitted and absorbed in small packages, which where given the name quanta. Albert Einstein took Plancks postulate even further. Einstein said that these quanta where really particles and with this he was able to explain the photoelectric effect. At the time, Bohr had explained the discrete spectrum of the hydrogen atom by invoking classical mechanics, although he had to quantize the angular momentum. More than a decade later Schrödinger took the ideas floating around and published his wave equation.
Solid state physics is concerned with describing the behavior of large solids from their microscopic properties. In solids, atoms are bond through electromagnetic forces, often in a periodic structure which is called a crystal lattice. The Schrödinger equation has been solved analytically only for the simplest atom, the hydrogen atom, where we have two bodies. As soon as we introduce another body, consider helium, the Schrödinger equation can not be solved analytically. The complexity and rich physical behavior of solids comes from the many-body character of many phenomena in solids, i.e. the interaction of multiple bodies at the same time. The complexity of the Schrödinger equation grows exponentially with the number of particles.
The complexity has been dealt with using various methods over the years. One early approach by Hartree and Fock is the Hartree-Fock approximation, which states that the wave function can be described by a single Slater determinant of all spin-orbitals in the system [1]. A more relevant approach for our purposes is Density Functional Theory (DFT). Moreover, DFT maps the complicated interacting system onto a non-interacting system with the same density [2]. The price of the simplification is that the potentials become more complicated.
Another method to simplify the many-body problem is to adopt a toy model, which still has most of the relevant physical properties. A common toy model for electrons in a periodic solid, is the Hubbard model: The model accounts for hopping between the nearest-neighbor

sites and Coulomb repulsion of two electrons at the same site. It can be visualized as a chain of hydrogen atoms where electrons are free to move between atoms, and whenever they are on the same site their energy is increased. In three dimensions the chain becomes a periodic grid of hydrogen atoms. The relevant physical property that is kept is the correlation between electrons. The Hubbard model exhibits a Mott-insulator phase transition, which is a quantum phase transition from conducting to insulating behavior. However, the phase transition makes the model an interesting toy model. The Hubbard model has gained traction, since it has been shown to exhibit high temperature superconductivity [3]. High temperature superconductivity is a long unsolved mystery in solid state physics, nevertheless high temperature superconductors are becoming increasingly popular in industry. The one-dimensional Hubbard model has been solved using the Behte-ansatz in 1968 by Lieb and Wu [4, 5].
In order to include the effects of vibrations in the solid, we consider the Hubbard-Holstein(HH) model. The HH model expands the Hubbard model to include phonons, which are quasiparticles for the quantization of vibration. Phonons are similar to photons which are the quanta of the electromagnetic field, however, photons are not actually quasiparticles.
Thermodynamics was developed during the 19th century, as a way to optimize thermal engines. It is a theory about exchange of energy between macroscopic objects, however, other quantities can of course also be exchanged. There are four fundamental laws of thermodynamics, if we include the so-called zeroth law. The motivation for the laws came from experiments, but they where later formalized into laws of nature. As for almost all physical theories, there where some problems when thermodynamics was first founded. One of the founding fathers of thermodynamics, Maxwell, devised a paradox called Maxwell's demon. Imagine that we have a box filled with a gas, which is divided up in two compartments by an impermeable wall. The wall can be opened or closed at will by the demon. Now, assume the demon knows the position and velocity of all particles in the box. The demon opens the wall whenever a particle with high speed is traveling towards the right compartment and whenever a particle with low speed is traveling towards the left compartment the demon opens the wall. Otherwise, the demon keeps the wall closed. After some time, the particles will be sorted, with the fast particles in the right compartment and the slow particles in the left compartment. The right compartment is now a hot reservoir and the left is a cold reservoir. The paradox violates the first law of thermodynamics, as useful work can be extracted from the hot reservoir [6].
The resolution to the paradox came from information theory, when Landauer proposed that information is physical. Maxwell's demon needs to keep the information about the particles in its memory, what is more, the information needs to be updated whenever a particle changes trajectory. Storing information does not require any work, but erasing one bit of information requires a minimum work of $k_B T \log(2)$ [7].
Stochastic thermodynamics is a natural extension to thermodynamics, which describes the non-equilibrium regime of thermodynamics. Often, for small systems where fluctuations are important. The random thermal fluctuations in stochastic thermodynamics are induced by a thermal bath, which is coupled to the system. We imagine that the system follows a well defined path in phase space determined by an external controller, but the system changes discontinuously at some points due to thermal fluctuations. Thus, the stochastic changes are identified as the heat and the smooth changes from the well defined protocol is the work. In stochastic thermodynamics there are many fluctuation relations, these describe how

probability densities fluctuate in non-equilibrium states or how the non-equilibrium processes are related to equilibrium parameters. Some of the fluctuation relations have been extended to closed quantum systems, in particular the Crooks relation and the Jarzynski equality have been extended to the quantum realm [8]. Stochastic thermodynamics deals with nano-scale systems, while Quantum thermodynamics deals with quantum-scale systems.
At the quantum scale there are both quantum mechanical and thermodynamic fluctuations. The "quantumness" and the fluctuations comes from the few available energy levels, along with the fact that we are far from the thermodynamic limit [9]. There are some effects that are intrinsically quantum, which need to be considered, such as coherence and entanglement. In particular, what happens if we meassure the system? Then it should, by the postulates of quantum mechanics, collapse into one of its eigenstates. Using the process of measurement to drive an engine is currently being studied. There are also ideas on how information can be used to drive an engine [6].
The development of the field of quantum thermodynamics(QTD) is driven by the increasing demand for smaller devices in the semiconductor industry [10]. Within QTD there exists several formalisms to describe heat and work, nonetheless in this thesis only the "standard" formalism will be used. The standard formalism is, in some sense, the simplest. However, when the system is divided up into parts, the shift in energy due to the interaction is not included explicitly in the expression for energy in each of the parts. Then one needs to include an artificial "interaction energy", with for example the Energy-Flux formalism the interaction energy is partially included in each of the parts [11]. When the system is divided in parts in section 3.2, we have an artificial interaction energy. However, the interaction energy will be negligible in our case.
Putting all these elements together gives us the chance to do QTD in an electron-phonon system. For the system we are considering here, this has never been done before to our knowledge. We use a simple lattice model for electrons and phonons, which still has interesting physics. We hope to be able to extract some qualitative trends in QTD from the HH dimer we are using. To this end, we use Exact diagonalization (ED), the Suzuki-Trotter(ST) decomposition and the Lanczos method. The system is prepared in various states, by putting different parts of the system in contact with a thermal bath, or preparing a non-equilibrium state. Time evolution is either done by changing the interaction parameters, these are the Hubbard $U$ and the electron-phonon coupling $g$, or by applying an external field $v_i(t)$.
In the present thesis only the exact solution is considered, however, our plan is to do a comparison with DFT in a future publication. The Ehrenfest approximation will also be considered, where the nuclei are treated classically [12, 13]. In our case, the nuclei are represented by phonons.

## 1.1 Lattice models

### 1.1.1 Hubbard model

John Hubbard proposed a simple model in 1963 to explain electronic correlations in narrow energy bands [14], of which we will present a more modern derivation here based on [15]. The starting point of the derivation is a non-relativistic Hamiltonian, which includes interactions between electrons. We employ the Born-Oppenheimer approximation, so the nuclei in the

solid are treated separately. In detail,

$$\begin{aligned} H &= H_{kin} + H_{ee} \\ &= \sum_{\sigma} \int d^3r\, \psi^{\dagger}_{\sigma}(\mathbf{r}) \left[ -\frac{\nabla^2}{2m} + U_{ion} \right] \psi_{\sigma}(\mathbf{r}) \\ &+ \sum_{\sigma,\sigma'} \int d^3r \int d^3r' \psi^{\dagger}_{\sigma}(\mathbf{r}) \psi^{\dagger}_{\sigma'}(\mathbf{r}') V(r-r') \psi_{\sigma'}(\mathbf{r}') \psi_{\sigma}(\mathbf{r}), \qquad V(r-r') \propto \frac{1}{|r-r'|}. \end{aligned} \tag{1.1}$$

The Hamiltonian in eq. (1.1) is the electronic "Theory of everything" in condensed matter physics. The Hamiltonian is written in terms of spin-orbit field operators $\psi_{\sigma}(\mathbf{r})(\psi^{\dagger}_{\sigma}(\mathbf{r}))$ that annihilate(create) electrons at position $\mathbf{r}$ with spin $\sigma$. We are working with a periodic lattice, therefore Bloch's theorem applies. Any wave function can be written as a product of a lattice periodic function $u_{\alpha}(\mathbf{r})$ and a phase $e^{i\mathbf{k}\cdot\mathbf{r}}$. The inverse Fourier transformed Bloch functions, i.e. the Wannier functions $\phi_R(\mathbf{r})$, is also used. The Wannier and Bloch functions are connected by a unitary transformation. The three previously mentioned objects are defined as:

$$\psi^{\dagger}_{\sigma}(\mathbf{r}) = \sum_{\mathbf{k}} \psi^{*}_{k}(\mathbf{r}) c^{\dagger}_{\mathbf{k}\sigma}, \qquad \psi_{\alpha\mathbf{k}} = u_{\alpha}(\mathbf{r}) e^{i\mathbf{k}\cdot\mathbf{r}}, \qquad \phi_{\mathbf{R}}(\mathbf{r}) = \frac{1}{\sqrt{N}} \sum_{\mathbf{k},\alpha} e^{-i\mathbf{k}\cdot\mathbf{r}} u_{\mathbf{k}\alpha}(\mathbf{r}), \tag{1.2}$$

with the corresponding inverse relations. Field operators are used to create, or annihilate, electrons in Wannier states. We also write the inverse relation:

$$\psi^{\dagger}_{\sigma}(\mathbf{r}) = \sum_{i\alpha} \phi^{*}_{i\alpha} c^{\dagger}_{\mathbf{i}\alpha\sigma}, \qquad\qquad c^{\dagger}_{\mathbf{i}\alpha\sigma} = \int d^3\mathbf{r} \phi_{i\alpha} \psi^{\dagger}_{\sigma}(\mathbf{r}). \tag{1.3}$$

The operators $c^{\dagger}_{\mathbf{i}\alpha\sigma}(c_{\mathbf{i}\alpha\sigma})$ obey the canonical anti-commutation relations for fermions and therefore act as creation(annihilation) operators. The Hamiltonian in eq. (1.1) written in the Wannier basis becomes

$$H = \sum_{\mathbf{ij}\alpha\beta\sigma} t^{\alpha\beta}_{ij} c^{\dagger}_{\mathbf{i}\alpha\sigma} c_{\mathbf{j}\beta\sigma} + \sum_{\mathbf{ijmn}} \sum_{\alpha\beta\nu\mu} \sum_{\sigma\sigma'} v^{\alpha\beta\nu\mu}_{\mathbf{ijmn}} c^{\dagger}_{\mathbf{i}\alpha\sigma} c^{\dagger}_{\mathbf{j}\beta\sigma'} c_{\mathbf{n}\nu\sigma'} c_{\mathbf{m}\mu\sigma} \tag{1.4}$$

the matrix elements $t^{\alpha\beta}_{ij}$ and $v^{\alpha\beta\nu\mu}_{\mathbf{ijmn}}$ are given by the overlap of the Wannier functions with the one-body and two-body operators in eq. (1.1) respectively. Now we start to make approximations to our still very general Hamiltonian. The only approximation done so far is the Born-Oppenheimer approximation. Assume that we are looking within one band, such that we can drop the indices $\alpha$,$\beta$,$\nu$ and $\mu$. Assume that the band is of $s$-type, furthermore this implies that the matrix elements are isotropic. Assume that matrix elements decrease fast enough, such that we can restrict the sums to the nearest-neighbors. The Wannier functions are well localized, in close analogy to molecular orbitals in atomic physics. These

three approximations applied to eq. (1.4) yield the generalized Hubbard model

$$
\begin{aligned}
H = & -t \sum_{\langle \mathbf{ij} \rangle \sigma} (c^{\dagger}_{\mathbf{i}\sigma} c_{\mathbf{j}\sigma} + h.c.) + \sum_i \epsilon_i \hat{n}_i \\
& + U \sum_{\mathbf{i}} \hat{n}_{\mathbf{i}\uparrow} \hat{n}_{\mathbf{i}\downarrow} + V \sum_{\langle \mathbf{ij} \rangle} \hat{n}_{\mathbf{i}} \hat{n}_{\mathbf{j}} + J \sum_{\langle \mathbf{ij} \rangle} \mathbf{S}_i \cdot \mathbf{S}_j \\
& + X \sum_{\langle \mathbf{ij} \rangle \sigma} (c^{\dagger}_{\mathbf{i}\sigma} c_{\mathbf{j}\sigma} + h.c.)(\hat{n}_{\mathbf{i}-\sigma} + \hat{n}_{\mathbf{j}-\sigma}) + Y \sum_{\langle \mathbf{ij} \rangle \sigma} (c^{\dagger}_{\mathbf{i}\uparrow} c^{\dagger}_{\mathbf{i}\downarrow} c_{\mathbf{j}\uparrow} c_{\mathbf{j}\downarrow} + h.c.).
\end{aligned} \tag{1.5}
$$

Here, $\langle \mathbf{ij} \rangle$ means the sum is over nearest-neighbors, and the operators

$$
\hat{n}_{\mathbf{i}} = \hat{n}_{\mathbf{i}\uparrow} + \hat{n}_{\mathbf{i}\downarrow}, \qquad\qquad \hat{n}_{\mathbf{i}\sigma} = c^{\dagger}_{\mathbf{i}\sigma} c_{\mathbf{i}\sigma},
$$

have been introduced. The Hamiltonian in eq. (1.5) has terms corresponding to all the possible combinations of the nearest-neighbor elements. In the first row we have the one-body matrix elements, which are the hopping terms between the nearest-neighbors "t" and on-site energy $t_{ii} = \epsilon$. $\epsilon_i$ can be viewed as an external potential $v_i(t)$. Furthermore, the two-body matrix elements have four distinct possible combinations $v_{iiii}$, $v_{iiij}$, $v_{iijj}$, $v_{ijij}$, if we neglect spin. The distinct combinations of indices for nearest-neighbor matrix elements which contribute to the Hamiltonian in eq. (1.5) are shown in the table below, where we use the notation $(c^{\dagger}_{i\sigma}, c_{j\sigma}, c^{\dagger}_{m\sigma'} c_{n\sigma'})$, and where we have restricted the model to one dimension.

Table 1: The distinct combinations of creation and annihilation operators (Here, $\bar{\sigma} \equiv -\sigma$).

| | | | |
|---|---|---|---|
| $\epsilon(c^{\dagger}_{i\sigma}, c_{i\sigma}, c^{\dagger}_{i\sigma}, c_{i\sigma})$ | $V(c^{\dagger}_{i\sigma}, c_{i\sigma}, c^{\dagger}_{j\sigma}, c_{j\sigma})$ | $0(c^{\dagger}_{i\sigma}, c_{j\sigma}, c^{\dagger}_{i\sigma}, c_{j\sigma})$ | $0(c^{\dagger}_{i\sigma}, c_{j\sigma}, c^{\dagger}_{i\sigma}, c_{j\sigma})$ |
| $U(c^{\dagger}_{i\bar{\sigma}}, c_{i\bar{\sigma}}, c^{\dagger}_{i\sigma}, c_{i\sigma})$ | $V(c^{\dagger}_{i\bar{\sigma}}, c_{i\bar{\sigma}}, c^{\dagger}_{j\sigma}, c_{j\sigma})$ | $X(c^{\dagger}_{i\bar{\sigma}}, c_{j\bar{\sigma}}, c^{\dagger}_{i\sigma}, c_{i\sigma})$ | $Y(c^{\dagger}_{i\bar{\sigma}}, c_{j\bar{\sigma}}, c^{\dagger}_{i\sigma}, c_{j\sigma})$ |

The $\epsilon$ term appears since $\hat{n}^2_{i\sigma} = \hat{n}_{i\sigma}$ and two of the combinations above are zero, since two fermions are created in the same state. The $U$-term is the contact Coulomb repulsion, the $V$-term is the nearest-neighbor Coulomb repulsion, the $Y$-term is the hopping of electron pairs, the $X$-term is called the bond-charge interaction or density-dependent-hopping since it looks like hooping times the density, the $J$-term is the spin-spin interaction. Matrix elements for $J$ are not explicitly written in the table above, since when we expand $\hat{\mathbf{S}}_i \cdot \hat{\mathbf{S}}_j = \frac{1}{2}\hat{S}_{+,j}\hat{S}_{-,i} + \frac{1}{2}\hat{S}_{-,i}\hat{S}_{+,j} + \hat{S}_{z,i}\hat{S}_{z,j}$ they appear in many of the other terms. The last approximation is now done, we drop all the terms except $U$, since this term gives the largest contribution [14]. Let us write the simplified Hamiltonian $H_H$,

$$
H_H = -t \sum_{\langle ij \rangle \sigma} (c^{\dagger}_{i\sigma} c_{j\sigma} + h.c.) + \sum_i v_i(t) \hat{n}_i + U \sum_i \hat{n}_{i\uparrow} \hat{n}_{i\downarrow}. \tag{1.6}
$$

The Hamiltonian in eq. (1.6) is the Hubbard Hamiltonian, after this point we will use the notation $J = t$ to not confuse $t$ with time. The Hamiltonian in eq. (1.6) is written for an arbitrary one dimensional chain, however, we will be working with two sites only. One striking feature is that there is a negative sign on the first term, however, there is no reason to expect a negative sign. In fact, the negative sign is a convention. The convention is useful, as

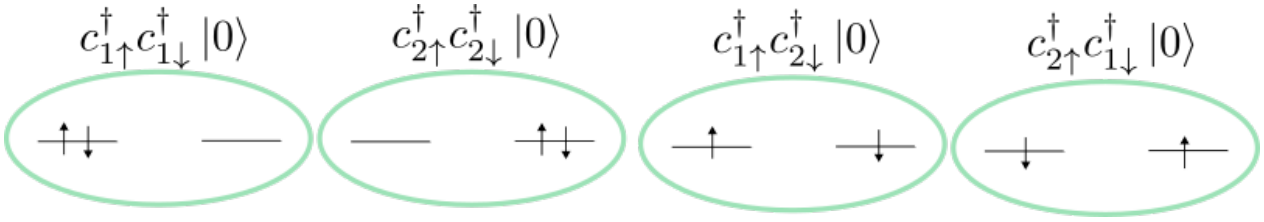


Figure 1: The basis states of the Hubbard dimer at half-filling.

the first term is often negative. A positive $t$ corresponds to an energy band with a maximum at $k = 0$, therefore the energy decreases with increasing $k$. One may expect that the energy increases with $k$, since $k$ is similar to momentum. We will consider a band, which is perhaps more natural, that has increasing energy as a function of $k$ and therefore we insert a minus sign in front of $t$.
We will confine ourselves to a dimer at half-filling in this thesis. A dimer is a system of two sites. The terminology is adapted from chemistry, where dimers are two molecules bond together. Half-filling means that the system has half of the maximum number of particles, in our case of a dimer the maximum number of particles is four. There are two sites that can have two electrons with opposite spin each, so the maximum is indeed four. If we consider a system of four particles, then the dynamics is not very interesting, since nothing can move. If we consider a system of three particles, then two must have the same spin and two of the particles can not move. Therefore, the problem reduces to a one-particle problem. The only situation which is not a one-particle problem is the half-filling case and therefore this case is chosen. There are four possible configurations of electrons in the dimer at half-filling (see Fig. 1), these will be used as our basis states in calculations.

### 1.1.2 Hubbard-Holstein model

Electron-phonon interactions are ubiquitous in solid state physics. Phonons play a role in the conducting properties of most materials, superconductivity is a striking example of the importance of electron-phonon interactions. Optical properties of materials is another area which displays the importance phonons, since when there is no direct band gap a phonon needs to be produced(or destroyed) to conserve momentum [16]. Holstein introduced his model to study polarons [17]. A polaron is a fermionic quasiparticle, which was invented to model the interaction between electrons and atoms in a solid. Holstein considered a physical situation where an electron was moving slowly through a molecular crystal. In the physical situation, the interactions between lattice and electrons become important. Holsteins model does not include the Hubbard interaction $U$, if this is included then we get what is called the Hubbard-Holstein model:

$$\begin{aligned} H_{HH} &= H_H + H_{ph} + H_{e-ph} \\ &= -J\sum_{\langle ij\rangle\sigma}(c^\dagger_{i\sigma}c_{j\sigma} + h.c.) + \sum_i v_i(t)\hat{n}_i + U\sum_i \hat{n}_{i\uparrow}\hat{n}_{i\downarrow} \\ &+ \sum_i(\omega b^\dagger_i b_i + \sqrt{2}\eta\,\hat{x}_i) + \sqrt{2}g\sum_i(\hat{n}_i - 1)\hat{x}_i. \end{aligned} \tag{1.7}$$

Here, $b_i^\dagger(b_i)$ is the creation(annihilation) operator for a phonon with frequency $\omega$ at site $i$, $\sqrt{2}\hat{x}_i = b_i + b_i^\dagger$ is the linear stretch of the spring in the oscillator that represents the phonon at site $i$ and $\eta$ is some external stretch of the spring. We only consider one frequency for all phonons and the frequency $\omega$ is fixed, such that there is no dispersion. An important feature of the HH Hamiltonian is that it contains both attractive and repulsive many-body interactions, where $g$ is attractive and $U$ is repulsive. It is not immediately obvious that the electron-phonon interaction $g$ is attractive. The attractive interaction is a result of performing a Lang-Firsov transformation on eq. (1.7) [18, 19]. The transformation, from $H$ to $\tilde{H}$, is a unitary transformation. We start by defining the transformation

$$\tilde{H} = e^{i\hat{S}} H e^{-i\hat{S}}, \qquad \hat{S} = \frac{\sqrt{2}}{\omega}\sum_i \hat{p}_i(g[\hat{n}_i - 1] + \eta), \qquad \hat{p}_i = \frac{i(b_i^\dagger - b_i)}{\sqrt{2}}. \tag{1.8}$$

The calculation is done through the Baker-Hausdorff lemma [20]:

$$\tilde{H} = e^{i\hat{S}} H e^{-i\hat{S}} = \sum_{n=0}^{\infty} \frac{i^n}{n!} \underbrace{[\hat{S}, [\hat{S}, .., [\hat{S}, [\hat{S}}_{n:th\ commutator}, H]...]]]. \tag{1.9}$$

The lemma can be proved by induction. Performing the calculation in eq. (1.9), we get

$$\tilde{H} = \sum_i \tilde{v}\hat{n}_i + \tilde{U}\hat{n}_{i\uparrow}\hat{n}_{i\downarrow} - \sum_{\langle ij\rangle}(\tilde{J}_{ij}c_i^\dagger c_j + h.c.) + \sum_i \omega \tilde{b}_i^\dagger \tilde{b}_i - \frac{(\eta - g)^2}{\omega}, \tag{1.10}$$

where new renormalized parameters have been introduced. These parameters are defined as:

$$\begin{aligned} \tilde{U} &= U - \frac{2g^2}{\omega}, \\ \tilde{v} &= v + \frac{g^2}{\omega} - \frac{2g\eta}{\omega}, \\ \tilde{J}_{ij} &= Je^{i\sqrt{2}(\hat{p}_i - \hat{p}_j)/\omega}. \end{aligned}$$

Here, $\hat{p}$ is the momentum operator defined in eq. (1.8), by the mathematical form of $\tilde{J}_{ij}$ it is a translation operator. The zeroth term in the expansion eq. (1.9) is the original Hamiltonian, therefore the transformed Hamiltonian has some terms left from to the original Hamiltonian. The factor $\frac{2g^2}{\omega}$ in $\tilde{U}$ brings down the energy for double occupation, if $g$ is large enough then double occupancy will be favored. $\tilde{v}$ yields an extra term $\frac{g^2}{\omega}$ on each of the sites that have phonons. From these arguments we define a parameter $\lambda = \frac{g^2}{\omega}$, which is the scaling factor for the effective strength of the electron-phonon interaction.
The HH model in eq. (1.7) is homogeneous. In this thesis we will consider two alterations of the HH model, both are inhomogeneous, since there are more intricate effects in inhomogeneous models. The first alteration is to collapse the sum in the final term of eq. (1.7) and set $\eta = 0$:

$$\begin{aligned} H_{HH} &= H_H + H_{ph} + H_{e-ph} \\ &= -J\sum_{\langle ij\rangle\sigma}(c_{i\sigma}^\dagger c_{j\sigma} + h.c.) + \sum_i v_i(t)n_i + U\sum_i n_{i\uparrow}n_{i\downarrow} \\ &+ \sum_i \omega b_i^\dagger b_i + \sqrt{2}g\,(\hat{n}_1 - 1)\,\hat{x}_1. \end{aligned} \tag{1.11}$$

We call (1.11) and (1.12) inhomogeneous HH Hamiltonians. Another possible flavor of the model is to remove the vacuum term (i.e. the minus one) in the electron-phonon coupling:

$$\begin{aligned} H_{HH} &= H_H + H_{ph} + H_{e-ph} \\ &= -J \sum_{\langle ij \rangle \sigma} (c^\dagger_{i\sigma} c_{j\sigma} + h.c.) + \sum_i v_i(t) \hat{n}_i + U \sum_i \hat{n}_{i\uparrow} \hat{n}_{i\downarrow} \\ &+ \sum_i \omega b^\dagger_i b_i + \sqrt{2} g \, \hat{n}_1 \, \hat{x}_1, \end{aligned} \tag{1.12}$$

which yields a slightly different Hamiltonian. We now only have one phonon mode in the system, so we call $\hat{x}_1 = \hat{x}$. Classically, the term $g\hat{n}_1\hat{x}$ can be both positive and negative, since the spring can be stretched both negatively and positively. To see the attraction quantum mechanically, observe that $\langle x \rangle = \mathrm{Tr}(\rho x)$ is the weighted sum of the elements in the superdiagonal and subdiagonal in the phonon basis. The density matrix is Hermitian, so $x$ is real. However, the important point is that the off-diagonal elements are not necessarily positive, contrary to the diagonal elements. The off-diagonal elements are the overlap between different states and the diagonal elements are the overlap with the state itself.
There are four basis states for the Hubbard dimer at half filling, see Fig. 1. When phonons are introduced the basis grows to $4 \cdot (n+1)$, where $n$ is the maximum number of allowed phonons. If we set $n = 0$, then we have the ordinary Hubbard Hamiltonian. The matrix representation for the HH dimer Hamiltonian in eq. (1.12) is written below for $n = 1$.

$$\begin{pmatrix} U+2v_1 & J & J & 0 & 2g & 0 & 0 & 0 \\ J & v_1+v_2 & 0 & J & 0 & g & 0 & 0 \\ J & 0 & v_1+v_2 & J & 0 & 0 & g & 0 \\ 0 & J & J & U+2v_2 & 0 & 0 & 0 & 0 \\ 2g & 0 & 0 & 0 & U+2v_1+\omega & J & J & 0 \\ 0 & g & 0 & 0 & J & v_1+v_2+\omega & 0 & J \\ 0 & 0 & g & 0 & J & 0 & v_1+v_2+\omega & J \\ 0 & 0 & 0 & 0 & 0 & J & J & U+2v_2+\omega \end{pmatrix}$$

The basis states of the Hubbard dimer are

$$|\psi_1\rangle = c^\dagger_{1\uparrow} c^\dagger_{1\downarrow} |0\rangle \qquad |\psi_2\rangle = c^\dagger_{1\uparrow} c^\dagger_{2\downarrow} |0\rangle \qquad |\psi_3\rangle = c^\dagger_{2\uparrow} c^\dagger_{1\downarrow} |0\rangle \qquad |\psi_4\rangle = c^\dagger_{2\uparrow} c^\dagger_{2\downarrow} |0\rangle \tag{1.13}$$

and to get the HH dimer we introduce a tensor state $|\psi_i\rangle \otimes |n\rangle$, where $i = 1, 2, 3, 4$ and $n$ is the number of phonons in the system. The matrix is divided in 4×4 blocks, spanned by the four states in eq. (1.13), visualized in Fig. 1. The off-diagonal 4×4 blocks, that contain the $g$:s, correspond to the $g\hat{n}_1\hat{x}$-term. Overlap between the $|\psi_i\rangle \otimes |n\rangle$ and the $|\psi_i\rangle \otimes |n \pm 1\rangle$ states is due to the operator $\hat{x}$. $n$ can be any positive integer, however, in numerical calculations the basis is restricted.

## 1.2 The density matrix formalism

Consider an ensemble of states, for example, take the spin-states of an electron. The value of an observable must have a contribution from each of the states in the ensemble. In other

words, we may have an ensemble that is a mix of eigenstates to the operators $\hat{S}_x$ and $\hat{S}_y$. We write the expectation value for operator $\hat{A}$, as the average value in our ensemble:

$$\langle \hat{A} \rangle = \sum_i w_i \langle \alpha_i | \hat{A} | \alpha_i \rangle = \sum_{b'} \sum_b \sum_i \left( w_i \langle b' | \alpha_i \rangle \langle \alpha_i | b \rangle \right) \langle b | \hat{A} | b' \rangle , \tag{1.14}$$

where $w_i$ is the weight of a state in the ensemble, $|\alpha_i\rangle$ is a state in the ensemble, $|b\rangle$ and $|b'\rangle$ are arbitrary bases spanning the ket space. The mathematical form motivates the density matrix $\rho$, as the operator representation of the object within the parenthesis. In our example, the density matrix is a 2×2 matrix encoding the information of the mix of eigenstates to the operators $\hat{S}_x$ and $\hat{S}_y$. There may be an infinite number of spin-states, nevertheless the density remains 2×2 [20]. We define $\rho$ and $\langle \hat{A} \rangle$ as

$$\rho = \sum_i w_i |\alpha_i\rangle\langle\alpha_i| , \qquad \langle \hat{A} \rangle = \mathrm{Tr}(\rho \hat{A}) = \sum_{b'} \sum_b \langle b' | \rho | b \rangle \langle b | \hat{A} | b' \rangle . \tag{1.15}$$

The "quantumness" of the density matrix is in the off-diagonal elements. If the density matrix is diagonal, then there is no overlap between the basis vectors and the density matrix representation is unnecessary. The off-diagonal elements are coherences in the quantum state, which give the correlations between the states. Coherences are what makes the quantum state interfere with itself, such as in the double slit experiment. In particular, imagine that the ensemble interacts with the environment. The perturbation from the environment is expected to be such that the system interacts randomly with the atoms in the environment, furthermore these perturbations must drive the system closer to a state stable from the perturbation. In effect, the perturbations collapse the off-diagonal elements in the density matrix and the probability distribution becomes classical. The phenomena of going from an inherently quantum probability distribution, to a classical one is known as decoherence. This does not explain the mechanism behind the collapse of the wave function, however, closer study of quantum statistical mechanics may lead to an explanation of this long-standing question. [21] The density matrix obeys the following equation of motion, as can be seen by taking the derivative of $\rho$,

$$\frac{\partial \rho}{\partial t} = \sum_i w_i \left( \frac{\partial |\alpha_i\rangle}{\partial t} \langle \alpha_i | + |\alpha_i\rangle \frac{\partial \langle \alpha_i |}{\partial t} \right) = -i/\hbar H\rho + i/\hbar \rho H = -i/\hbar [\rho, H]. \tag{1.16}$$

The $\hbar$ will be omitted in calculations, since we use $\hbar = 1$, although it is used here to clarify that the Schrödinger equation has been used to arrive at the equation of motion. The probability of an eigenstate being occupied is its weight. The statistical weight $w_i$ is not quantum mechanical, it is simply the fraction of the population in a state. However, if the density is expanded in an eigenbasis $\{|b\rangle\}$ corresponding to the operator $\hat{A}$ in eq. (1.15), then the probability of obtaining an eigenvalue $b_i$ from the state $\alpha_i$ is $|\langle b_i | \alpha_i \rangle|^2$. This is the Born rule, which is at the heart of quantum mechanics. In quantum statistical mechanics $w_i$ has a special meaning, it is identified as the thermodynamic weight of each state, the Gibbs-factor. Nevertheless, $w_i$ is still a classical weight. Normalizing the density matrix corresponds to that the sum of weights is one, which means that the trace is one. We identify the normalizing factor as the partition function, since

$$\rho = \sum_i w_i |\alpha_i\rangle\langle\alpha_i| = \sum_\lambda \frac{e^{-E_\lambda \beta}}{Z} |\lambda\rangle\langle\lambda| = \frac{e^{-H\beta}}{Z} , \qquad Z = \mathrm{Tr}\big(e^{-H\beta}\big). \tag{1.17}$$

Time evolution of the density matrix can also be given in terms of the time evolution operator $\mathcal{U}(t, t_0)$, all the states building up the density matrix evolve with the same $\mathcal{U}(t, t_0)$. Therefore, the total matrix time evolves with the same operator

$$\rho(t) = \mathcal{U}(t, 0)\rho(0)\mathcal{U}(t, 0)^\dagger. \tag{1.18}$$

## 1.3 Quantum Thermodynamics

In QTD we are working systems that have few degrees of freedom and a small amount of particles. Due to the restriction of the system, we are far from the thermodynamic limit. Therefore, there are both thermal fluctuations and quantum fluctuations that need to be considered. In contrast to normal thermodynamics, where the uncertainty comes from the thermal fluctuations only. Furthermore, heat and work are not observables, as one would naively expect, they are stochastic variables [22, 23]. In this thesis, we confine ourselves to the so-called standard framework [11], which we now introduce. The internal energy is given by

$$U = \mathrm{Tr}(\rho H). \tag{1.19}$$

Consider that the internal energy changes a small amount in a small time interval $\mathrm{d}t$, that is

$$\mathrm{d}U = \mathrm{Tr}\left(\frac{\mathrm{d}\rho}{\mathrm{d}t}H\right)\mathrm{d}t + \mathrm{Tr}\left(\rho\frac{\mathrm{d}H}{\mathrm{d}t}\right)\mathrm{d}t, \qquad \Delta U = \mathrm{Tr}(\rho(\tau)H(\tau)) - \mathrm{Tr}(\rho(0)H(0)). \tag{1.20}$$

The change in the total energy $U$ is the difference between the starting and end point, which means that it is a function of state. We compare eq. (1.20) to the first law of thermodynamics from conventional thermodynamics for infinitesimal transformations

$$\mathrm{d}U = \delta Q + \delta W, \tag{1.21}$$

and we can identify the terms

$$\Delta U = \langle Q\rangle + \langle W\rangle, \qquad \langle Q\rangle = \int_0^\tau \mathrm{d}t\,\mathrm{Tr}\left(\frac{\mathrm{d}\rho}{\mathrm{d}t}H\right), \qquad \langle W\rangle = \int_0^\tau \mathrm{d}t\,\mathrm{Tr}\left(\rho\frac{\mathrm{d}H}{\mathrm{d}t}\right). \tag{1.22}$$

The given definition of heat and work is conceptually sound, as it is consistent with the first law of thermodynamics. We have identified the work performed on the system as the change in energy due to changes in the Hamiltonian and the heat absorbed by the system as the change in energy due to changes in the density matrix. No work can be done if the Hamiltonian does not change with time and similarly if the density matrix is constant, then there is no heat produced. If the system is closed, then we expect zero heat. Moreover, the lack of heat is reflected in the equation of motion for the density matrix in eq. (1.16) and the cyclic property of the trace:

$$\langle Q\rangle = \int_0^\tau \mathrm{d}t\,\mathrm{Tr}\left(\frac{\mathrm{d}\rho}{\mathrm{d}t}H\right) = \int_0^\tau \mathrm{d}t\,\mathrm{Tr}(-i[H,\rho]H) = 0. \tag{1.23}$$

However, if the system is divided up in parts, heat can flow between them. Note that we use the opposite sign convention in this thesis, $\langle W\rangle = -\int_0^\tau \mathrm{Tr}\big(\rho\frac{\mathrm{d}H}{\mathrm{d}t}\big)\mathrm{d}t$, as we interested in the work performed by the system and therefore we also change the sign of the heat.

# 2 Method

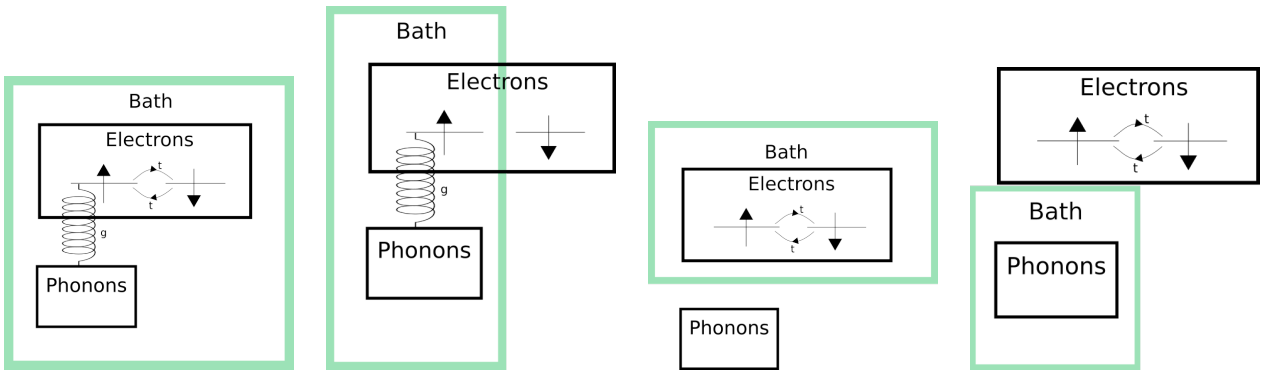


Figure 2: A few ways to prepare the system before the dynamics. Only a) and b) are presented in this thesis, however, the other cases have also been considered.

We prepare our system in contact with a thermal bath at $t < 0$, some examples on how this can be done is given in the figures above. If the whole system is not connected to the bath, then the initial state is a factorized state $\rho_{Bath} \otimes \rho_{System}$. The density matrix for the bath is given by eq. (1.17), as $\rho_{Bath} = \frac{e^{-\beta H_{Bath}}}{Z}$. However, if the whole system is prepared in a bath, then the initial state is not factorized, it is simply given by $\rho_{Bath}$. We time evolve the density matrix at $t > 0$ through eq. (1.18), with the full Hamiltonian. During the time evolution either an external field $v_i(t)$ is applied on the electrons, or the couplings $U$ and $g$ are changed. We defer to the appendix for additional plots showing how we change the parameters as a function of time. The hopping parameter $J$ is used as the energy unit. The unit of time is $\hbar/J$. Results are presented in terms a dimensionless quantity, representing the physical units multiplied by $J/\hbar$.

## 2.1 Time evolution

The time evolution of the system is done through the time evolution operator $\mathcal{U}(t, t_0)$. The operator $\mathcal{U}$ evolves a ket from $t_0$ to $t$. $\mathcal{U}(t, t_0)$ obeys a Schrödinger-like equation [20],

$$i\hbar \frac{\partial}{\partial t}\mathcal{U}(t, t_0) = H\mathcal{U}(t, t_0). \tag{2.1}$$

For small time intervals $\Delta$, we can assume that the Hamiltonian is time independent and then the solution is an exponential. We write,

$$\mathcal{U}(t + \Delta, t) = e^{-iH\cdot(t+\Delta-t)/\hbar} = e^{-iH\cdot\Delta/\hbar}. \tag{2.2}$$

To increase the accuracy, a trapezoidal rule is used by diagonalizing $H(t + \Delta/2)$ to find $H(t + \Delta/2)\,|\lambda\rangle = E_\lambda\,|\lambda\rangle$, instead of $H(t)$. Doing the procedure for the time interval $[0, T]$, with $\Delta = \frac{T}{N}$, we obtain a solution for $\mathcal{U}$:

$$\mathcal{U}(T, 0) = \lim_{N\to\infty} \prod_{n=1}^{N} e^{-i/\hbar H((n-1)\Delta+\Delta/2)\cdot\Delta} = \lim_{N\to\infty} \prod_{n=1}^{N} \sum_{\lambda} e^{-i/\hbar E_\lambda\cdot\Delta}\,|\lambda\rangle\langle\lambda|\,. \tag{2.3}$$

The full solution, if the Hamiltonian does not commute with itself at different times, is a Dyson series. Time evolution through exact diagonalization (ED) is done by picking a large enough $N$ and diagonalizing $H(t + \Delta/2)$ at each time step. However, as the Hamiltonian matrix gets large the computation becomes costly. The time complexity scales like $\mathcal{O}(M^3)$, with a simple divide and conquer algorithm [24], where $M$ is the size of the matrix.

### 2.1.1 The Suzuki-Trotter decomposition

If we know that some parts of the Hamiltonian does not depend on time, we can make approximations [25]. The Suzuki-Trotter(ST) decomposition is an approximation to the sum of two matrices in an exponential:

$$e^{(H+V)x} = e^{(V/2)x} e^{Hx} e^{(V/2)x} + \mathcal{O}(x^3). \tag{2.4}$$

We use the second-order expansion here. However, the formula can be extended to arbitrary order. The proof is done by expanding the right-hand side to second order in $x$ and then comparing it to the taylor-series for the left-hand side(LHS), thus

$$\begin{aligned}
&\left(I + \frac{V}{2}x + \left(\frac{V}{2}\right)^2 \frac{x^2}{2}\right)\left(I + Hx + H^2\frac{x^2}{2}\right)\left(I + \frac{V}{2}x + \left(\frac{V}{2}\right)^2 \frac{x^2}{2}\right) + \mathcal{O}(x^3) \\
&= I + \frac{V}{2}x + \left(\frac{V}{2}\right)^2 \frac{x^2}{2} + Hx + H^2\frac{x^2}{2} + x^2 H\frac{V}{2} + \frac{V}{2}x + \left(\frac{V}{2}\right)^2 x^2 + \frac{V}{2}Hx^2 \\
&+ \left(\frac{V}{2}\right)^2 \frac{x^2}{2} + \mathcal{O}(x^3) = I + x(H+V) + \frac{x^2}{2}(H+V)^2 + \mathcal{O}(x^3) = \text{LHS} + \mathcal{O}(x^3).
\end{aligned}$$

If $x$ is a small number the approximation is good, for our purposes $x = i\Delta$. The ST decomposition is better than a simpler power series method, since it keeps unitarity.

### 2.1.2 The Lanczos method

In the version of the Lanczos method that is considered in this thesis we start with a wave function $|\phi_0\rangle$ and find an easier matrix problem to solve [26], explicitly:

$$|\Phi_1\rangle = (1 - |\phi_0\rangle\langle\phi_0|)H\,|\phi_0\rangle\,, \qquad \alpha_0 = \langle\phi_0|H|\phi_0\rangle\,, \qquad \beta_1^2 = \langle\Phi_1|\Phi_1\rangle\,. \tag{2.5}$$

We have found a state orthogonal to the original state by using a projection operator $P_0 = |\phi_0\rangle\langle\phi_0|$. However, $\beta_1$ is also a matrix element:

$$H\,|\phi_0\rangle = |\Phi_1\rangle + |\phi_0\rangle\,\langle\phi_0|H|\phi_0\rangle \implies \langle\phi_1|H|\phi_0\rangle = \langle\phi_1|\Phi_1\rangle = \beta_1. \tag{2.6}$$

The key point of the Lanczos method comes when we construct the next vector in the sequence:

$$|\Phi_2\rangle = (1-P_1)(1-P_0)H\,|\phi_1\rangle = (1-P_1-P_0)H\,|\phi_1\rangle = H\,|\phi_1\rangle - \alpha_1\,|\phi_1\rangle - \beta_1\,|\phi_0\rangle\,. \tag{2.7}$$

By the same reasoning as before, we get the matrix elements $\alpha_2 = \langle\phi_2|H|\phi_2\rangle$ and $\beta_2 = \langle\phi_1|H|\phi_2\rangle$, however $\langle\phi_0|H|\phi_2\rangle = 0$:

$$\langle\phi_0|H|\phi_2\rangle = (\langle\Phi_1| + \alpha_0\,\langle\phi_0|)\,|\phi_2\rangle = 0, \tag{2.8}$$

by the construction the kets $|\phi\rangle$:s are always orthonormal. The basic pattern above holds to all orders of $|\phi_M\rangle$. We write the Hamiltonian with the sequence $\{|\phi_0\rangle, |\phi_1\rangle, |\phi_2\rangle, \dots\}$ to get a tridiagonal matrix. Numerically, one cuts of the sequence at a vector $|\phi_M\rangle$. The time evolution is done by diagonalizing the reduced matrix. The benefit of the Lanczos is that the tridiagonal matrix is usually much smaller than the original Hamiltonian, therefore it is much faster to diagonalize. Tridiagonal matrices are also easier to diagonalize, since there are faster algorithms to diagonalize Tridiagonal matrices. Often tridiagonalization is an intermediate step in diagonalization.

## 2.2 Computational details

The codes developed and used for this project were written in FORTRAN, using a pre-existing code as initial template. From the template I wrote the remaining code myself, including the data analysis, which was performed in Python. All the results presented in the thesis come from calculations on the Vespa cluster, where we used the first ten nodes. However, these nodes where of varying quality (see appendix C). Finally, the time evolution algorithms described above are suitable for parallel computing, and this turned out to be necessary, to have execution times of the order of days/weeks (rather than considerably longer).

# 3 Results and Discussion

## 3.1 Adiabaticity versus Coulomb repulsion

Adiabatic processes are important in thermodynamics, therefore the competition between the Hubbard $U$ versus the length of the time evolution $\tau$ is analyzed. We use an inhomogeneous HH dimer Hamiltonian at half-filling (See eq. (1.11)). The time evolution is done with the ST decomposition in this section. The dynamics starts from thermal equilibrium with the whole system in a thermal bath, as in eq. (1.17) and Fig. 2a. We set the Parameters to $\hbar\omega/J = 0.1$, $k_BT = 1/\beta = 0.2J$ and $v_i(t)$ now also depends on $\tau$:

$$v_i(t)/J = (-1)^{i+1}\left(1 + 7\sin\left(\frac{\pi t}{2\tau}\right)\right). \tag{3.1}$$

The system evolves in the time interval $[0, \tau]$, note that $\tau \times J$ is the adiabaticity measure. One noticeable thing in eq. (3.1) is that $v(0) \neq 0$, in effect, the initial state favors site 2. For $g/J = 0.3$ the phononic energy is $\lambda/\hbar J = 0.9$, therefore the phonons dominate the dynamics for small $U/J < 0.9$, conversely for $g/J = 0$ the Hamiltonian reduces to the Hubbard Hamiltonian in eq. (1.6). The thermal energy $k_BT = 0.2J$ is quite small, therefore the initial state has a negligible contribution from excited states and the ground state gives the main contribution to the dynamics. The final work is minus the change in internal energy, since the system is closed.

We first focus only on the electronic effects, see Figs. 3a), 3b). See Figs. 12a, 12b for higher resolution of 3a),3b). The computational cost is much higher when introducing phonons, so naturally the heat maps contains fewer data points when $g/J \neq 0$. The external field drives the system towards double occupation at site 2, while the Hubbard $U$ decreases double occupation. The spectrum of the Hamiltonian is gaped, moreover, the gap is $0.39 \leq \Delta E/J \leq 2.82$ between the ground state and the first excited state [22]. Notice that the gap is a function of $U$.

For small $\tau \times J/\hbar \sim 1$, i.e. in the first column of the heat maps (where $\tau \times J/\hbar = 1$), the system does not have time to react to the external field and therefore the work is mainly due to the change in the Hamiltonian. The regime $\tau \times J/\hbar \sim 1$ is called sudden-quench. On the other side of the heat map, the behavior is adiabatic. Adiabatic means that the eigenstates of the Hamiltonian in the ensemble remain eigenstates of the Hamiltonian at all times, although the eigenvalues may change. Of course our process is not perfectly adiabatic at $\tau \times J/\hbar = 10$, although it is a useful way of thinking. The system needs to be driven through an anticrossing when $\Delta E$ and $U$ is large, essentially population can not be transferred between sites.

For large enough $U$ the Hubbard model exhibits the precursor of the Mott-insulator phase transition, as the system goes from conducting to insulating[1]. Less work is extracted for larger $U$:s, since the applied field becomes less effective, due to the phase transition. When phonons are included, the characteristic features in $n_1$ are smoothed out and the work is constant for a large regime, see Figs. 3d), 3e) and 10a, 10b. It seems like most of the rich physical behavior disappears, especially in the density at site 1. Above a certain threshold

[1]Strictly speaking, a phase transition happens in the thermodynamic limit. Therefore in our very small system it is only possible to talk about behavior which is the finite-size version of the behavior observed in a bulk sample. For ease of language, we henceforth refer to it as "precursor" behavior.

$U/J \gtrsim 4$, the qualitative behavior is the same as for $g = 0$. $U/J \gtrsim 4$ can be compared to the energy scale for the phonons $\lambda/J\hbar \approx 1$. However, the analogy with $\lambda$ can not be pushed to far, as $\lambda$ is only the scaling factor for the renormalized parameters and the Lang-Firsov transformed system is not the same as the original Hubbard model.

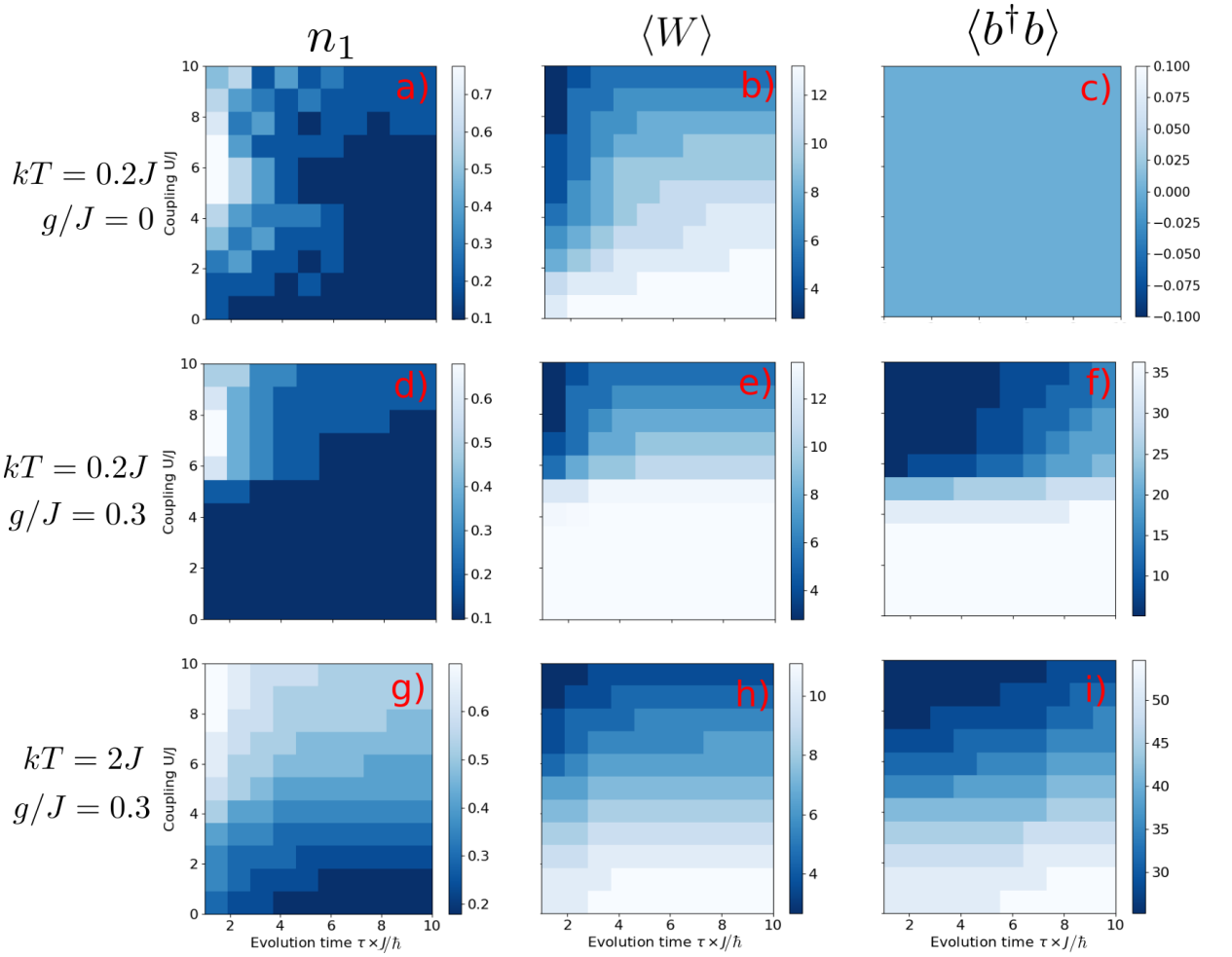


Figure 3: Contour plots at $t = \tau$ of the electron density at site 1 $n_1$ (left), the work $\langle W \rangle$ (middle) and the phonon occupation number $\langle b^\dagger b \rangle$ (right). On the x-axis the degree of adiabaticity is reported and the y-axis refers to the interaction strength $U/J$. Here, $\hbar\omega/J = 0.1$, we increase the thermal energy $kT$ and the electron-phonon coupling $g$, from top to bottom. The phonons are detached from the system in c), as a result the phonon occupancy $\langle b^\dagger b \rangle$ is zero everywhere.

In a schematic picture at $T = 0$, for low $U$ and when $g \neq 0$, the presence of phonons lowers the energy compared to the phononless case. Pictorially, this is because the spring is stretched towards negative values, such that $g \langle (\hat{n}_1 - 1)\hat{x} \rangle$ brings down the energy, and the electronic density increases on site 1. This stretch comes at a cost, since the contribution of the $\omega$-term increases, and a compromise must be reached. Furthermore, increasing the electron density at a site 1 implies an increased larger repulsion term $U\langle n_{1\uparrow} n_{1\downarrow} \rangle$. For higher $U$, the density is more evenly distributed and phonons are less important in the initial state, nevertheless

the above picture can also be applied in this case. At finite temperatures, the initial density matrix is a mixture of this state and higher energy excited states, and so the ground state is not the only state that contributes to the dynamics. Yet, it still plays a major role, due to it having the largest thermal weight.
When phonons are introduced, there is no limit on the available energy levels. Due to the bosonic nature of phonons, any number of phonons can be created. The energy levels are closely spaced, they are separated by $\hbar\omega = 0.1J$. The spacing in energy levels is smaller than the thermal energy $kT = 0.2J$, so excited states are easily accessible.
Intermediate-levels effectively remove the insulating phase for small $U$:s, hence there is no longer a gap. Compared to the case in which there are no phonons, Fig. 3e), the field efficacy is not reduced for small $U$ in Fig. 3h). Rather, it remains constant. In the previous case we examined, the precursor of the Mott-insulator phase transition was responsible for a reduction of the work. Conversely, if there are not enough phonons, then the gap can not be bridged. The largest possible gap is $\Delta E = 2.82/J$, which corresponds to 28 phononic energy states in the gap. We can imagine that there is a ladder over the energy gap, which has steps of $\hbar\omega = 0.1J$. From the phonon occupation number in Fig. 3e), it is clear that for $U/J \lesssim 5$ the gap can be bridged.
It is interesting that site 1 gets almost completely depleted for $U/J \lesssim 3$, in Fig. 3d). Comparing Fig. 3d) to Fig. 3a), we see that depleting is the main effect when we introduce phonons.
In Figs. 3g) to 3i), the thermal energy has been increased up to $kT = 2J$. The thermal energy increases the number of phonons, since more excited states are accessible. The initial thermal bath also has more energy, which means that there are more phonons in the initial state. The dynamics at these parameters is clearly dominated by phonons.
Previously, in the pure Hubbard case, there were subtle effects, such as anticrossing, which blocked the transfer between sites. This lead to that density at site 1 was not correlated with the work. However, now $\langle W \rangle$ and $n_1$ look qualitatively like inverses of each other. In the colder case, see Figs. 3d) and 3e), the work is qualitatively the inverse of the density at site 1 for $U/J \lesssim 4$. In the pure Hubbard case, this regime is even smaller, there it holds approximately for $U/J \lesssim 1$ . Because the work is the inverse of the density at site 1, there is nothing hindering the transfer of energy from the external field to the system. The only thing affecting the work is the density. In other words, energy is easily stored and transferred within the system. The energy that would have been wasted in the pure Hubbard case is now stored in the system by creating many phonons.
For low $U$, the double occupancy on site 1 is favored in the initial state, as the attractive phonon potential can overcome the initial external potential. However, as the potential is applied, it creates a gap of $\Delta v/J = 16$. It is almost impossible to overcome the energy difference, so that site 2 is always favored in the final state. If the system is trapped at the second site, then there needs to be 160 steps of $\hbar\omega$ to transverse the gap in energy. Furthermore, the attractive electron-phonon potential is on the energy scale $\lambda/J\hbar = 0.9 \ll 16$, so that does not have an effect. In the low $U$ regime, the electrons start quite evenly distributed and are then driven to site 2. The effect becomes even more pronounced for larger $\tau \times J/\hbar$, as the final state is closer to the eigenstate of the final Hamiltonian. The density matrix for the eigenstates of the final Hamiltonian is dominated by site 2, since it has much less energy.

For high $U$, site 1 is still available in the initial state. Due to the attractive phonon potential and the large Hubbard $U$ blocking double occupation at both sites, the population of electrons is evenly distributed. The energy blocking double occupation on the second site is maximum at $U + \lambda/\hbar \approx 11J$(cfr. $\Delta v = 16J$), for $U = 10J$, so the energy scales are similar in the high $U$ regime. Nevertheless, we see that the effect of letting the system evolve for longer times $\tau$ is to transfer population to site 2. In this regime, the work done by the external field does not produce many phonons, see Fig. 3i). Most of the energy supplied to the system through the external potential is needed to overcome $U$, so not much of the energy is used to create phonons.

## 3.2 A phonon battery

In this section we consider how a splitting between left and right site can be used as a battery. The Hamiltonian is split up between left and right site, such that energy can flow between its parts. We prepare the initial state with one thermalized electron at the left site and one electron at the right site as in Fig. 2b. The left site is coupled to the phonons through a coupling $g(\hat{n}_1 - 1)\hat{x}$ (i.e., henceforth the left site is labeled by "1"). We let the system evolve with the Hamiltonian in eq. (1.11), through the Suzuki-Trotter decomposition. We set the parameters to $\hbar\omega = 0.1J$, $kT = 0.5J$, $U = 2J$, $g = 0.1J$, $v_i(t)/J = 10(-1)^{i+1}\sin\left(\frac{\pi t}{10}\right)$ and whenever the parameters are changed it is indicated in the plot. In the bottom right plot, we indicate the quantity $v_1(t)/J$ with $V(t)$. We summarize the splitting of the system at $t = 0$ mathematically as

$$\rho(0) = \left(\sum_{n=0}^{\infty} e^{-n\omega\beta} \left|n\right\rangle\!\left\langle n\right|\right) \otimes \left(c^{\dagger}_{L\downarrow} c^{\dagger}_{R\uparrow} \left|0\right\rangle\!\left\langle 0\right| c_{L\downarrow} c_{R\uparrow}\right), \tag{3.2}$$

where the initial state is written as $phonon \otimes electron$. At $t > 0$ the system evolves with the full hamiltonian, which is now split up into parts:

$$H(t > 0) = H_L^{(e+ph)} + I^{(ph)} \otimes H_R^{(e)} + H_{int}, \qquad U_{tot} = U_L + U_R + U_{int}. \tag{3.3}$$

The dimension of each subspace is given by their superscript, $\dim(H) = 4 \cdot n, \dim(H_L^{(e+ph)}) = 4 \cdot n, \dim(I^{(ph)}) = n, \dim(H_R^{(e)}) = 4, \dim(H_{int}) = 4 \cdot n$. The internal energy of each subsystem is obtained by a partial trace over that subsystem.

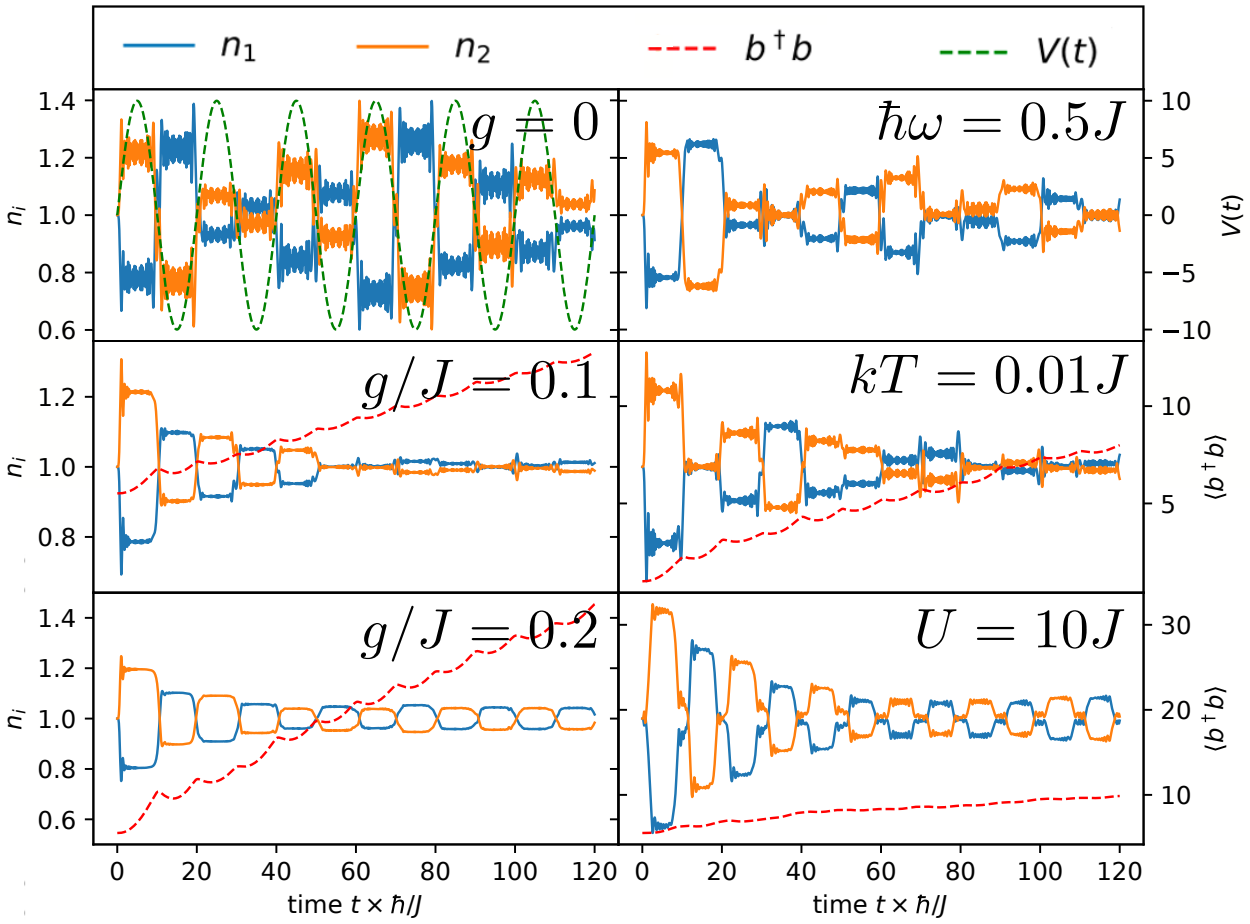


Figure 4: The phonon battery under various conditions, the parameter that is changed is indicated in the plot. For the top two plots $\langle b^\dagger b \rangle$ is not displayed, since there are no phonons for $g = 0$ and almost no phonons for $\hbar\omega = 0.5J$.

Table 2: The total energy before the dynamics and the distribution of energy after the dynamics.

| | $g/J = 0.1$ | $kT/J = 0.01$ | $g/J = 0.2$ | $U/J = 10$ | $\hbar\omega/J = 0.5$ | $g/J = 0$ |
|---|---|---|---|---|---|---|
| $U_L(120)$ | $1.52J$ | $1.08J$ | $3.11J$ | $2.16J$ | $1.35J$ | $0.82J$ |
| $U_R(120)$ | $0.30J$ | $0.29J$ | $0.31J$ | $1.40J$ | $0.30J$ | $0.44J$ |
| $U_{tot}(0)$ | $0.55J$ | $0.10J$ | $0.55J$ | $0.55J$ | $0.79J$ | $0.55J$ |
| $\Delta U = -\langle W \rangle$ | $1.28J$ | $1.27J$ | $2.85J$ | $3.02J$ | $0.92J$ | $0.69J$ |

The system in Fig. 4 has very rich physical behavior. The first thing to acknowledge is that without any phonons and external field, the double occupation fluctuates on both sites. The fluctuation of the double occupancy $\langle n_{i\uparrow} n_{i\downarrow} \rangle$ can be seen as the quantum mechanical vacuum fluctuations. The external field $v_i(t)$ is so large that it effectively freezes the electrons on their respective sites and when the potential crosses zero, some electrons tunnel over to the other site. The effect can be seen best in the pure electron case, i.e. the lower right panel of

Fig. 4. The fluctuations are smoothed out when $g \neq 0$, since phonons are created instead. Phonons are mainly created when the densities are trapped and some are dissipated when population is transferred between sites. The increase is roughly $\langle b^\dagger b \rangle \sim t$, which can be viewed as the charging speed of the battery. However, the $g = 0.2J$ case charges faster than the $g = 0.1J$ case, which is not surprising, since the coupling is larger. The coupling $g$ to the fluctuating electrons is what creates the phonons, so a larger coupling means a larger possibility of energy transfer.
In the bottom left panel we have a bottleneck behavior, since the fluctuations do not impart enough energy to transverse the energy gap of $\hbar\omega = 0.5J$. The energy levels are further apart in this regime. However, $g/J = 0.1 \ll 0.5 = \hbar\omega/J$, so it is less favorable to create phonons compared to when $\hbar\omega = 0.1J$. Furthermore, in the top panels we see that the temperature of the initial thermal bath only contributes with an additive factor in the phonon occupation number $\langle b^\dagger b \rangle$. From these two facts, we can conclude that it is not the thermal energy that charges the battery over time, it is really the transfer from external field to the electrons and then finally: to the phonons.
The interaction energy is negligible, it has a small numerical value. By the splitting of the system at $t < 0$, we have $U_R(t < 0) = U_{int}(t < 0) = 0$. The shape of the perturbation $v_i(t)$ is such that $\langle W \rangle$ is zero for a constant density matrix, i.e. $v_i(t)$ is odd. We can draw a few naive conclusions from Table. 2, the last row displays the total work done on the whole system. The change in the total energy $\Delta U$, which equals minus the work, is increasing function of $g$. The thermal energy does not effect the work in the system. The work is an increasing function of $U$, however, this is due to electronic effects and not further charging of the battery. Finally, the work decreases with larger $\hbar\omega$, due to the bottleneck.
Charging the battery means in our case increasing the phonon occupation number. This, as we have seen, has a steady increase when we apply a perturbation. A secondary effect is the energy increase on the left site, due to the coupling to the phonons. In the usual electric battery, the internal energy is stored in electrochemical cells. Here, however, we store energy by creating many phonons, each with energy $\hbar\omega$. Such "charged" phonon bath could be coupled to another suitable system, putting it in an excited state. This excited state could be such that the electrons in it are experiencing a higher potential, thus behaving in practice as electrons under the action of an ordinary battery.

## 3.3 Paths in $U$-$g$ space

So far, we have changed physical parameters, but now we are interested in changing the interactions, something possible e.g. in ultracold gases. Explicitly, we consider a path in $U$, which is the electron-electron repulsion and $g$, which is the electron-phonon interaction. In particular, imagine that we prepare a system with $U = g = 0$. If we create many phonons by increasing $g$, then the electrons will tend to occupy the site with phonons, therefore double occupation will be favored. However, if we increase $U$, then double occupancy will not be favored. In this way we expect a path dependence, similar to classical thermodynamics.

We consider three paths in $U$-$g$ phase space. The first path is linear, which means $U$ and $g$ change at the same rate from $U = 0$, $g = 0$ to $U = 3.6J$ and $g = 0.6J$. The other two paths are sinusoidal, they start and end at the same points as the linear path, however, one of the variables follows a sinusoidal path. The three paths are displayed in Fig. 5, with $g$ as a function of $U$, i.e. $g(U)$. The system starts in a thermal state to the complete Hamiltonian in eq. (1.12) at $t < 0$ (See Fig. 2a), with $U = 0$, $g = 0$, $\hbar\omega = 0.1J$, $kT = 0.2J$, $v_i(t)/J = 0$ and the time evolution is done through the HH Hamlitonian with coupling $g\hat{n}_1\hat{x}$ as in eq. (1.12).

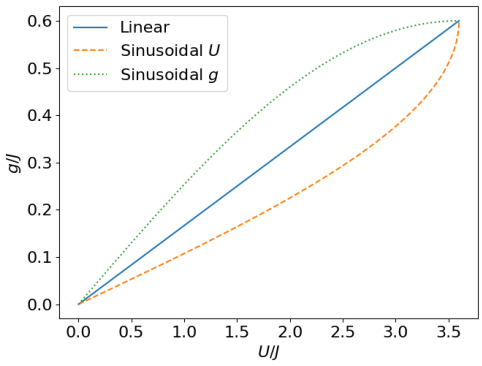


Figure 5: The three different paths in $U$-$g$ phase space that are considered in the main text.

The evolution of $U$ and $g$ is done for 10 units of time. See appendix B.3. for plots $U(t)$ and $g(t)$. Explicitly, the parameters changes as:

$$\begin{aligned} U(t)/J &= 0.36t \times J/\hbar & g(t)/J &= 0.06t \times J/\hbar, \\ U(t)/J &= 3.6\sin(\pi t/20) & g(t)/J &= 0.06t \times J/\hbar, \\ U(t)/J &= 0.36t \times J/\hbar & g(t)/J &= 0.6\sin(\pi t/20), \end{aligned}$$

for the linear, the sinusoidal in $U$ and the sinusoidal in $g$ path respectively. The system is isolated, therefore $\Delta U = -\langle W \rangle$. In the bottom right panel of Fig. 6, $\langle W \rangle$ is displayed as a function of time, which is always negative, so work is done on the system. The largest amount of work is required when we take a sinusoidal $g$ path, however, the other paths would need more work if the dynamics is cut of earlier. More work is required because the system spends longer time at higher $g$-values, which allows for a higher stretch of the spring and the producing of more phonons.

The system does not have time to react to the change of parameters. If it did have time to react, then we would have a more complicated behavior of the phonon number $\langle b^\dagger b \rangle$ and the electron density $n_1$. In this path, the occupation numbers are almost pure exponential functions. We usually see such simple behaviors when parameters are changed fast or extremely slow. The phonon time scale is given by $J/\hbar\omega = 10$, it is the same as the total time 10. In other words, we are in the sudden quench regime. On a slower path, we expect the displacement $\langle \hat{x} \rangle = \langle b + b^\dagger \rangle$ to oscillate.

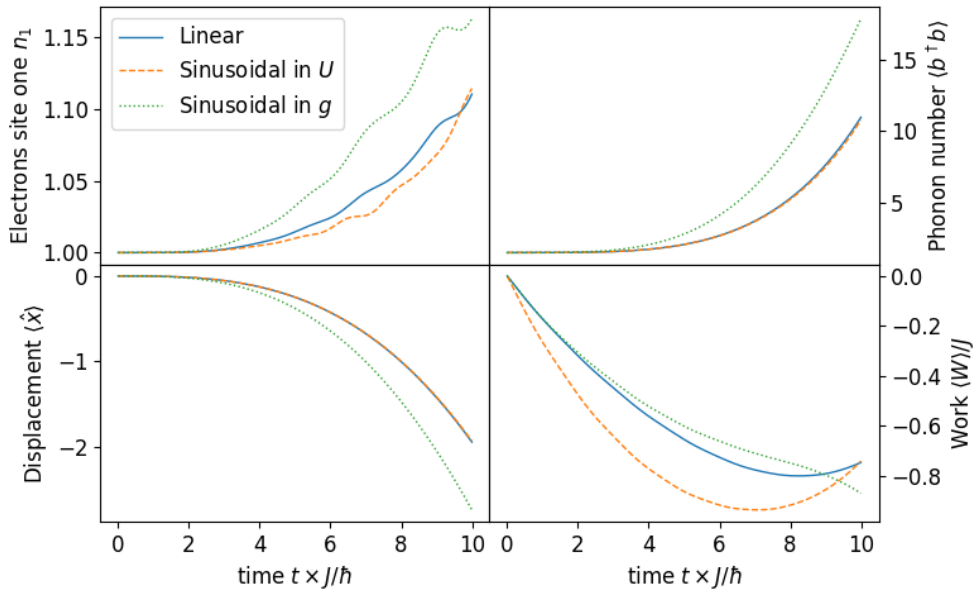


Figure 6: The three paths through phase space. Here, $\hbar\omega = 0.1J$, $kT = 0.2J$ and the whole system is prepared in a thermal bath. Notice that the work for all paths almost converges at the end of the dynamics, since $Ug$ converges.

The phonon number and phonon displacement is the same for the linear path and the sinusoidal $U$ path, since $g$ changes in the same way for both of them and therefore the electron-phonon interaction is the same. However, there are some differences in the electronic behavior, due to $U$. A small difference in the final electron occupation number at site 1 can be seen and there is a minuscule difference in work, $\langle W \rangle_{Lin}(t = 10\hbar/J) - \langle W \rangle_{SinU}(t = 10\hbar/J) = -0.006J$. If we take a path that includes $U/J \gtrsim 5$ and small $g$ values, then we will see the effect of the precursor of the Mott-insulator phase transition. Previously in section 3.1, we saw that $g = 0.6J$ removed the phase transition for $U/J \lesssim 5$ values.
At the end of the dynamics $\langle W \rangle$ is increasing for the linear path and the sinusoidal $U$ path, as the $g\hat{n}_1\hat{x}$ term starts to dominate the $\hbar\omega$:s. If we would let the system evolve for longer times, then the term $\hat{x}$ will oscillate. Oscillations will also lead to the increase of $\langle W \rangle$ in the sinusoidal $g$ path eventually.

## 3.4 Hysteresis in thermodynamic cycles

As complement to the study of thermodynamic paths, we look at thermodynamic cycles to see what happens within QTD in our electron-phonon system. Classically, thermodynamic cycles are done via e.g. Carnot cycles. In Carnot cycles, heat is exchanged between reservoirs, which produces work. Here, we give/take energy to/from the system by moving in the $Ug$-phase space and we then calculate the work. Since we already observed a battery behavior in our system (which somehow implies that the system has "memory"), we expect to see some irreversibility related to the fact that phonons are not conserved, and therefore we anticipate the occurrence of hysteresis

We consider a thermodynamic cycle in the Hubbard $U$ and the electron-phonon coupling $g$ plane. Thus, in the case of what we call an $Ug$-cycle: $U$ is increased from 0 to $1.6J$, $g$ is increased from 0 to $0.4J$, $U$ is decreased from $1.6J$ to 0, and finally $g$ is decreased from $0.4J$ to 0. For a $gU$-cycle: $g$ is increased from 0 to $0.4J$, $U$ is increased from 0 to $1.6J$, $g$ is decreased from $0.4J$ to 0 and finally $U$ is decreased from $1.6J$ to 0. The cycles are done slowly or fast, and the initial state is thermalized for high or low temperature.

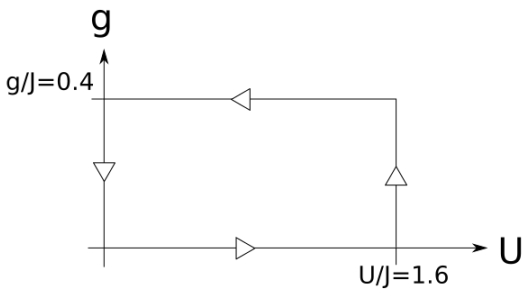


Figure 7: Phase space representation of the $Ug$-cycle.

We use an inhomogeneous HH dimer Hamiltonian with coupling $gn_1x$ (See eq.(1.12)) at half-filling and time evolve through the Lanczos method. The parameters are set as $\hbar\omega = 0.1J$, $v_i(t)/J = 0$ and the whole system is in a thermal bath for $t < 0$, as in Fig. 2a. The phase space parameters are increased and decreased linearly. However, there are many other ways one can imagine to increase and decrease the parameters. One can, for example, imagine that $g$ increases whenever the density on site 1 is high, this scheme would give a large work. In general, the optimal way to change the parameters is given by optimal control theory [27]. The shape of the "optimal control", which is the parameter that is changed, is often not obvious. However, we will not do optimal control theory in this thesis. Instead, for a $Ug$-cycle we change $U$ and $g$ as:

$$g(t)/J = \begin{cases} 0, & \text{if } t < \tau \\ 0.4\frac{t}{\tau}, & \text{if } \tau < t < 2\tau \\ 0.4, & \text{if } 2\tau < t < 3\tau \\ 0.4(1-\frac{t}{\tau}), & \text{if } \tau < t \end{cases}, \qquad U(t)/J = \begin{cases} 1.6\frac{t}{\tau}, & \text{if } t < \tau \\ 1.6, & \text{if } \tau < t < 2\tau \\ 1.6(1-\frac{t}{\tau}), & \text{if } 2\tau < t < 3\tau \\ 0, & \text{if } \tau < t \end{cases},$$

where $\tau$ is the allowed time for each parameter change, the total cycle is for $4\tau$, see also Fig. 18. $\lambda = g^2/\omega$ is changed by changing $g$, moreover, both $\lambda/\hbar$ and $U$ are their maximum equal to $1.6J$. The fast cycle is done for 12 units of time, as there are three units of time given to each change in parameter. Similarly, the slow cycle is done for 40 units of time and each parameter change takes ten units of time. We have picked the maximum $g$ and $U$, such that $\lambda_{max} = U_{max}$, so that the strength of the two interactions is comparable. In the four $Ug$-cycles, see Fig. 8, the densities do not change much before $g$ is maximized. For a $Ug$-cycle, the system has site symmetry when $g = 0$, so the two sites have the same behavior.

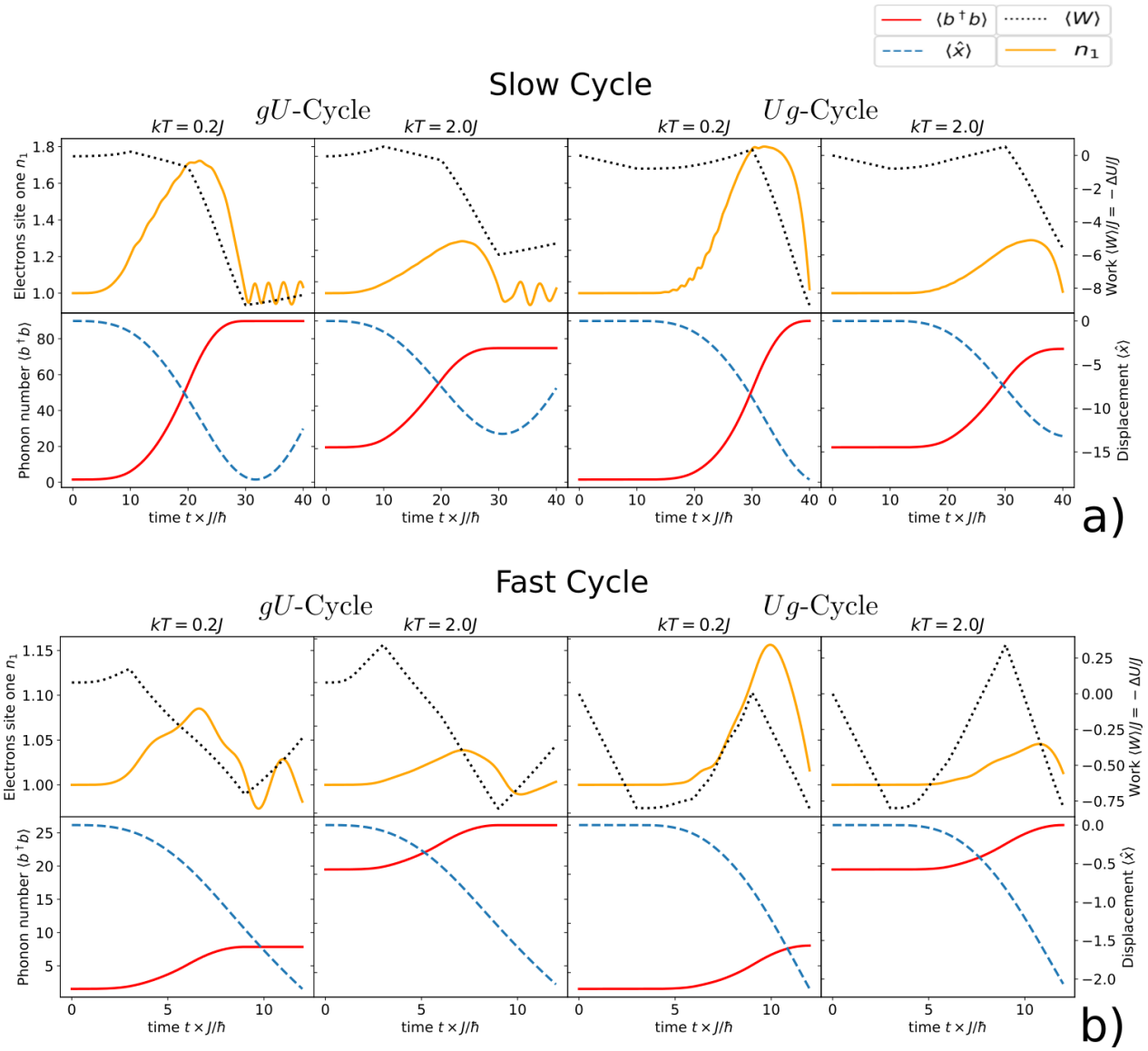


Figure 8: The eight cycles considered. In Panel a) $\tau = 10\hbar/J$, in b) $\tau = 3\hbar/J$. Here, $\hbar\omega = 0.1J$, all cycles start in thermal equilibrium at $t < 0$ with $U = g = 0$, then either a $Ug$-cycle or $gU$-cycle is performed. In the the columns, The thermal energy is alternating between $kT = 0.2J$ and $kT = 2.0J$.

Previously, in Fig. 3, the effect of including phonons was to deplete site 1. However, now the coupling is $g\hat{n}_1\hat{x}$, while previously it was $g(\hat{n}_1 - 1)\hat{x}$. The new coupling is only attractive towards site 1, $g(\hat{n}_1 - 1)x$ can be attractive towards site 2 and repulsive towards one if $n_1 < 1$. The coupling $g(\hat{n}_1 - 1)\hat{x}$ can also favor site 2, but we did not see this in section 3.1, since the system was prepared with an imbalance $v_i(0)/J \neq 0$. States that are stretched positively are always energetically unfavored with the coupling $g\hat{n}_1\hat{x}$. It is interesting to note that about half of the phonons are created when $g$ is constant, i.e. after $g$ has been increased to its maximum. In the graph $\langle b^\dagger b \rangle$ vs time, $g$ stops increasing at the inflection point. This delay is also seen in $\langle \hat{x} \rangle$.

The effect of the temperature is to smoothen the features in the electron density $\langle \sum_\sigma c_{1\sigma}^\dagger c_{1\sigma} \rangle = n_1$, in the phonon number $\langle b^\dagger b \rangle$ and the phonon displacement $\langle \hat{x} \rangle$. For the fast cycle 8b), the work values cover a wider range of numerical values at higher temperature, in contrast to the slow cycle 8a) where we have the to opposite behavior. Furthermore, the final value of the work in 8b) is almost independent of temperature. However, in 8a) temperature has an effect. In the fast cycle, there are more phonons excited in the initial state and throughout the dynamics when temperature is increased. On the contrary, in the slow cycle, the colder case starts with less phonons in the inital state, although there are more phonons in the final state.

We conjecture that the dependence on temperature in the slower cycles comes from the presence of phonons. For lower temperatures we are closer to the ground state, where the energy minimization occurs via a large negative stretch of the oscillator coordinate, and many phonons are present. In the fast cycle this does not happen, because the parameters are to suddenly changed for the minimization to occur. We can do a quick estimate of the change in the internal energy, i.e. minus the work for our purposes, by taking the difference in phonon number $\Delta\langle b^\dagger b \rangle$ between initial state and final state. $\Delta\langle b^\dagger b \rangle$ is multiplied by $\hbar\omega$ to get the energy. Moreover, $n_1$ is about the same in the initial and final state, therefore $\hbar\omega\langle b^\dagger b \rangle$ is the dominating contribution. We see that the difference in phonon number is approximately $\Delta\langle b^\dagger b \rangle \approx 6$ for all of the fast cycles, while for the slow cycles $\Delta\langle b^\dagger b \rangle$ has noticeable dependence in temperature. These simple considerations seem to be consistent with the results of Fig. 8. However, a more in-depth verification and discussion is beyond the scope of this thesis.

It is also worth noting at this point that for the small portion of $Ug$-space we are covering in this study it is hard to see a path dependence. It can quite easily be seen when the parameter change $U(t)$ or $g(t)$ is discontinuous, since then $\langle W \rangle$ is also discontinuous. In all of the cycles, the density $n_1$ is peaked whenever $U$ is minimized and $g$ is maximized, yet $n_1$ always returns to a value close to its initial value of 1. There is hysteresis in the phonon behavior, since the spring $\langle \hat{x} \rangle$ is still stretched and the created phonons still remain when all parameters have returned to zero.

Notably, the energy increases considerably towards the end of the cycle. The reason is that the electron-phonon term $g\hat{n}_1\hat{x}$ is slowly turned off, since $g$ is decreased to towards zero. The spring is still stretched negatively at the end of the cycle, but it is detached. However, when this term has vanished the system still remembers what has happened to it. There are many phonons that have been created in the cycle, and these contribute to the total energy by factors of $\hbar\omega$. The phonon number $\left\langle b^\dagger b \right\rangle$ and the work $\langle W \rangle$ prove that we have hysteresis.

The work $\langle W \rangle$ is larger for the slow perturbation, since the system has more time to absorb the energy given to it by changing $U$ and $g$. The thermal equilibrium state for $U/J = 1.6$ and $g/J = 0.4$ contains $\sim 30$ phonons, which is a little bit less than what we have for the slow cycles, although it is more than what we have for fast cycles.

To summarize, we have explored the conditions for adiabaticity in our system and based on this we have chosen three specific numerical cases to study: a battery, a path through $Ug$-space and a cycle in $Ug$-space. The results show that i) phonons very often absorb a large portion of the energy in the system and then store it, to release it subsequently; ii) they drastically affect the time evolution of the system.

# 4 Conclusion and outlook

In this thesis, QTD has been explored in the context of a lattice model containing phonons. To our knowledge, QTD has never been studied before in a HH model, therefore the purpose of the thesis is mainly explorative. We briefly summarize the main results and discuss how further research can be done to expand our results.

The code developed allowed us to expand on previous QTD results for a pure Hubbard dimer [22]. For low temperatures, the qualitative effect is a shift in the energy scale $U/J$. Naively, one may expect that the dynamics is completely different when we have many new energy states. We have also seen that the features in the densities and the work become smoothed out when we add phonons. The result is not surprising, since we are approaching the continuum limit.

The idea to use phonons to store energy has been explored within this thesis. In practice, one can imagine a large crystal that is prepared in a thermal bath. Half of the crystal is molecular, such that it has Holstein sites, and the other half is a simple crystal, such that it has pure Hubbard sites. The solid is then put in an vacuum, such that the system is isolated, finally an alternating current is applied, and the battery gets charged. However, due to us using a dimer, there are finite-size effects. It is not clear at this stage how the characteristics found in the dimer with larger size, e.g. at which extent the population of electrons that tunnel back and forth might be transported away from the junction.

We have also considered some paths through $U$-$g$ space, where we saw that it was unfavorable to go along a path where $g$ is higher, since then more work is required to go between the two phase space points. However, the result is for a fast non-adiabatic change of the parameters, there might be different results if we consider slower speeds. We start the system from $U = 0$ and $g = 0$, although if we would start the system from for example $g/J = 0.1$ , then there are more phonons in the initial state.

The last scenario considered was a thermodynamic cycle, we were able to demonstrate that an HH dimer, in fact, can exhibit hysteresis. It was also shown that work performed at the end of the cycles was nearly independent of the order in which the parameters were varied. For more adiabatic cycles, the phonon contribution dominated, while for faster cycles the major contribution was due to the electron degrees of freedom.

In this thesis, we have not considered the high $g$ regime, as the maximum $g$ used is $g/J = 0.6$. The HH Hamiltonian can model phonon mediated superconductivity at high $g$, so these parameters will definitely give interesting physics. We have conducted preliminary tests to do thermodynamic cycles with $g/J = 1$, however, it turned out that it required a basis of $\approx$ 1000-2000 phonons. A basis of $\approx$ 1000-2000 implies a Hamiltonian matrix of size 4000-8000, and we need to time evolve 4000-8000 eigenstates with the Hamiltonian, this is left for future work.

We have not considered any approximations to the dynamics in this thesis. The methods used have all been checked for convergence, so these methods have provided us with a numerical exact solution. The plan for a future paper is to implement semi-classical Ehrenfest dynamics and time-dependent density functional theory [28]. Time dependent DFT is an in principle ab-inito method, however, almost always the so-called exchange correlation potential needs to be simplified. DFT is a most common method used for realistic calculations, as of now QTD is mainly done for small model systems [11, 22]. DFT would bring us much closer to a

real world implementation of QTD, as DFT is the standard tool to calculate most material properties, while the Ehrenfest approximation would allow us to explore more stringently the boundary between QTD and classical thermodynamics.

# References


[1]D. R. Hartree and W. Hartree, Proc. R. Soc. Lond. A **150**, 9–33 (1935).

[2]W. Kohn and L. J. Sham, Phys. Rev. **140**, A1133–A1138 (1965).

[3]A. S. Alexandrov, J Supercond **18**, 603–612 (2005).

[4]E. H. Lieb and F. Wu, Physica A **321**, 1–27 (2003).

[5]E. H. Lieb and F. Wu, Phys. Rev. Lett. **20**, 1445–1448 (1968).

[6]A. Auffèves, SciPost Physics Lecture Notes (2021).

[7]R. Landauer, IBM Journal of Research and Development, 183–191 (1961).

[8]S. Vinjanampathy and J. Anders, Contemporary Physics **57**, 545–579 (2016).

[9]K. E. Dorfman et al., Phys. Rev. E **97**, 042120 (2018).

[10]S. Deffner and S. Campbell, *Quantum Thermodynamics: An introduction to the thermodynamics of quantum information* (2019).

[11]D. D. Moro, "Quantum Thermodynamics of a Hubbard Chain Coupled to a Qubit", PhD thesis (University of Bologna, 2020).

[12]T. W. R. Delos J B and K. S. K, Phys. Rev.A **6**, 706 (1972).

[13]P. Ehrenfest, Z.Physik **45**, 455–457 (1927).

[14]J. Hubbard, Proc. R. Soc. Lond. A **276**, 238–257 (1963).

[15]H.-P. Eckle, *Models of Quantum Matter: A First Course on Integrability and the Bethe Ansatz.* (2019).

[16]J. Deslippe et al., Comput. Phys. Commun. **183**, 1269–1289 (2012).

[17]T. Holstein, Annals of Physics **8**, 325–342 (1959).

[18]I. G. Lang and Y. A. Firsov, JETP **16**, 1301 (1962).

[19]P. Helmer, "Density Functional Theory for the Hubbard-Holstein model", MA thesis (2018).

[20]J. J. Sakurai and J. Napolitano, *Modern Quantum Mechanics (2nd ed.)* (2017).

[21]H. D. Zeh, Found. Phys. **1**, 69–76 (1970).

[22]M. Herrera et al., Eur. Phys. J. B **91**, 248 (2018).

[23]P. Talkner et al., Phys. Rev. E **75**, 050102 (2007).

[24]J. J. M. Cuppen, Numer. Math. **36**, 177–195 (1980).

[25]N. Hatano and M. Suzuki, Lecture Notes in Physics **679**, 37–68 (2005).

[26]C. Lanczos, J. Res. Nat. Bureau of Standards **45**, 255–282 (1950).

[27]S. Ydman et al., EPL **123**, 47001 (2018).

[28]C. Verdozzi et al., Phys. Rev. Lett. **97**, 046603 (2006).

# A Extra heat maps

In this section $\hbar = 1$.

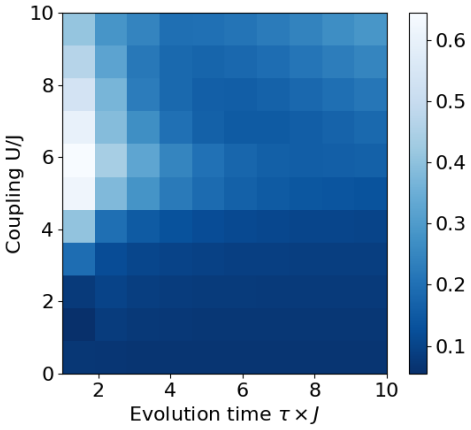


(a) $n_1$.

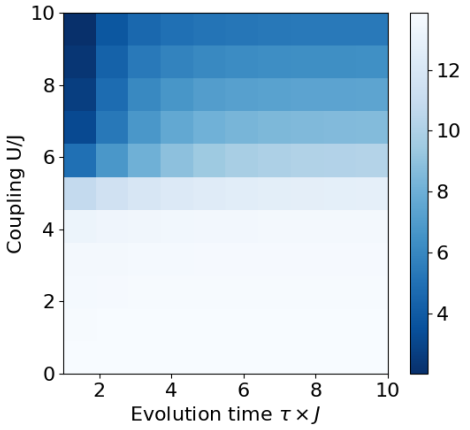


(b) $\langle W \rangle$.

Figure 9: $kT = 0.2J$, $g/J = 0.6$, not binned.

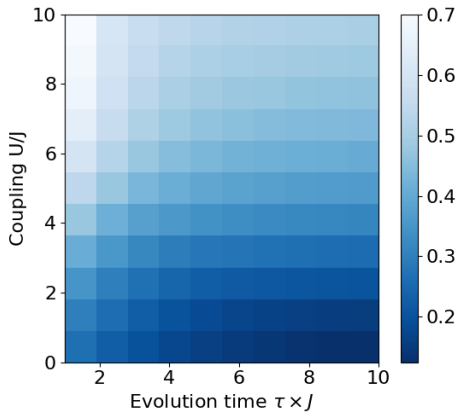


(a) $n_1$.

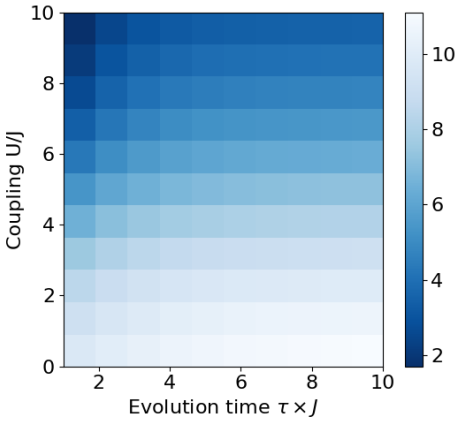


(b) $\langle W \rangle$.

Figure 10: $kT = 2.0J$, $g/J = 0.6$, not binned.

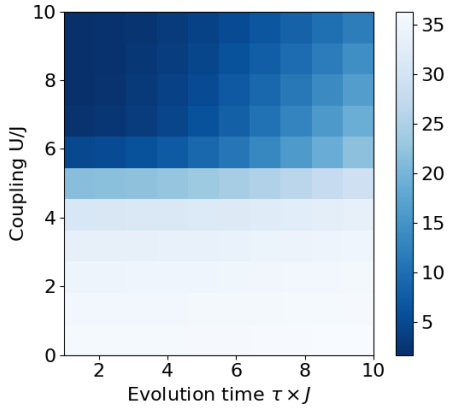


(a) $kT = 0.2J$.

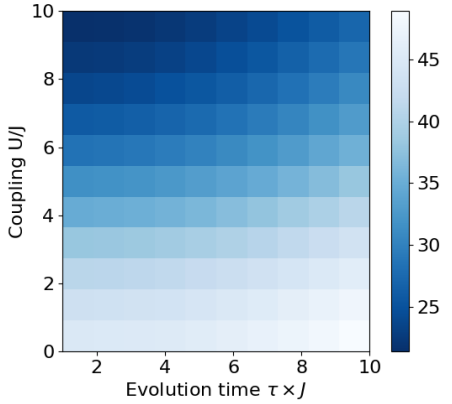


(b) $kT = 2J$.

Figure 11: The unbinned phonon occupation number, note the different scales.

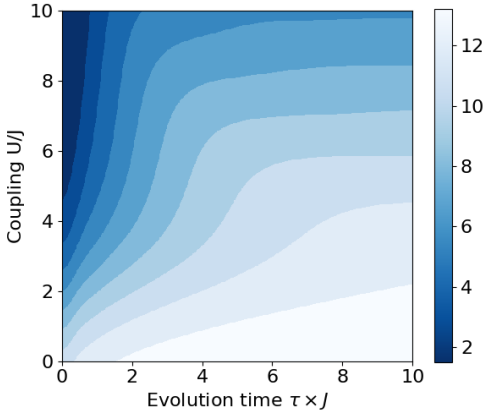


(a) $\langle W \rangle$.

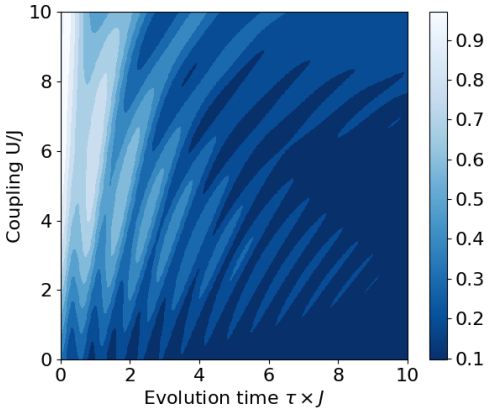


(b) $n_1$.

Figure 12: High resulotion plots for $g = 0$ and $kT = 0.2J$.

# B Plots of parameter changes vs. time

In this section time is measured in units of $\hbar/J$ and energy is measured in units of $J$.

## B.1 Adiabaticity versus Coulomb repulsion

$$v_i(t) = (-1)^{i+1}\left(1 + 7\sin\left(\frac{\pi t}{2\tau}\right)\right). \tag{B.1}$$

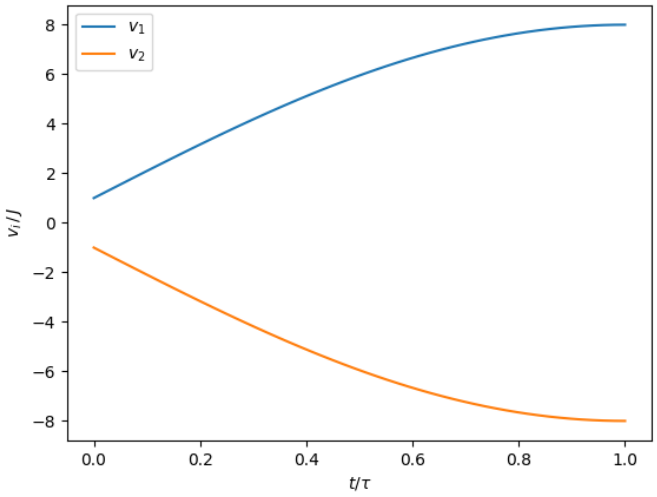


Figure 13: Potential

## B.2 The phonon battery

$$v_i(t) = 10(-1)^{i+1} \sin\left(\frac{\pi t}{10}\right) \tag{B.2}$$

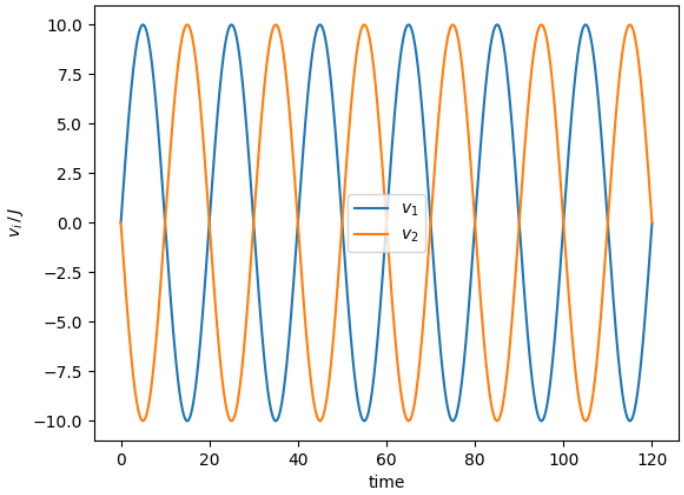


Figure 14: Potential

## B.3 Paths in $U$-$g$ space

The three paths are given as a function of time:

$$\begin{aligned} U(t) &= 0.36t & g(t) &= 0.06t, \\ U(t) &= 3.6\sin(\pi t/20) & g(t) &= 0.06t, \\ U(t) &= 0.36t & g(t) &= 0.6\sin(\pi t/20), \end{aligned}$$

which are the order: linear, sinusoidal in $U$ and sinusoidal in $g$.

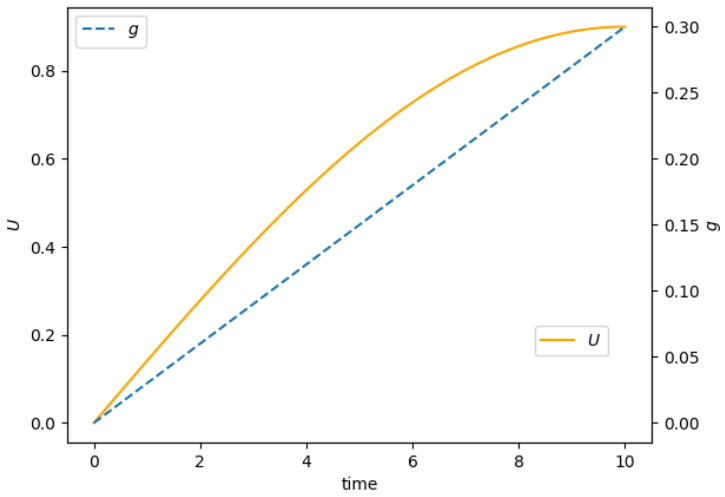


Figure 15: Sinusoidal in $U$

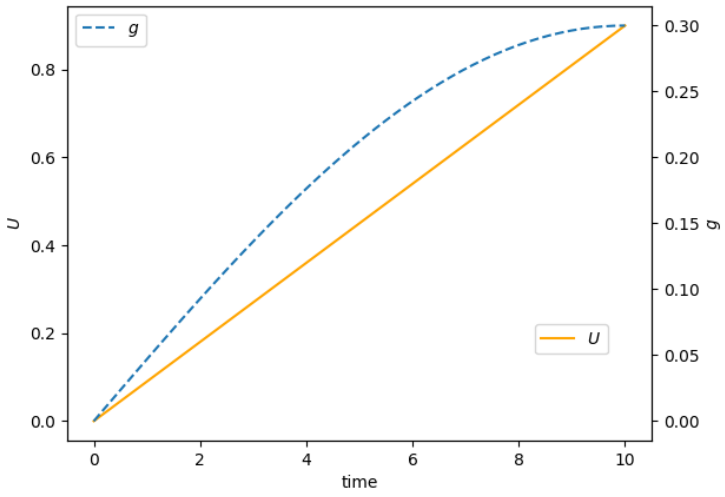


Figure 16: Sinusoidal in $g$

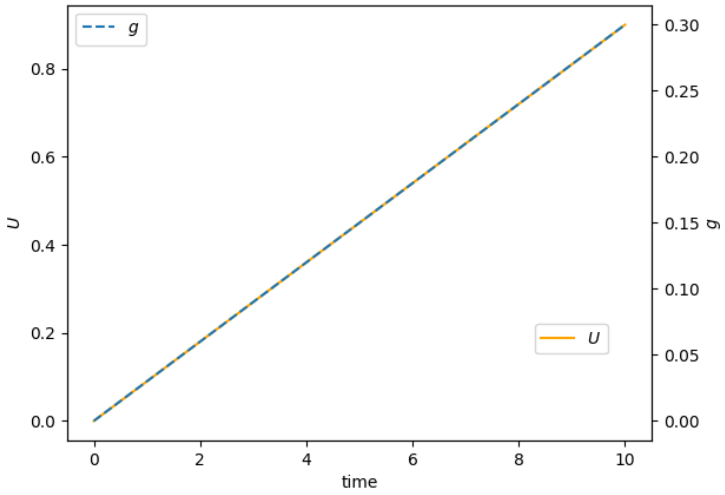


Figure 17: Linear in both parameters

## B.4 Hysteresis in thermodynamic cycles

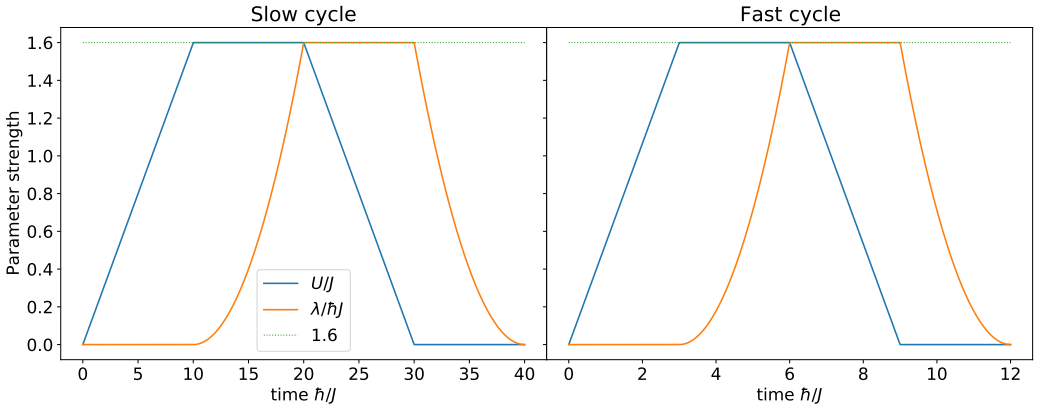


Figure 18: The fast and the slow $Ug$-cycle, if labels are exchanged ($U$ and $\lambda$) in the plot we get the $gU$-cycle. $\lambda = g^2/\omega$ and it is $g$ that changes $\lambda$, $\omega = 0.1$ is fixed

# C The nodes

Here are the relevant computer specifications for the nodes on the Vespa cluster that were used. Note that the first nodes are the best ones from the point of view of the performance.

| Node | 1 | 2 | 3 | 4 | 5 | 6 | 7 | 8 | 9 | 10 |
|---|---|---|---|---|---|---|---|---|---|---|
| CPUs | 16 | 16 | 16 | 16 | 16 | 16 | 8 | 8 | 8 | 8 |
| CPU MHz | 2534 | 2534 | 1600 | 1600 | 1600 | 1600 | 800 | 2300 | 800 | 800 |